International Journal of Pharmaceutics 609 (2021) 121188

Contents lists available at ScienceDirect

International Journal of Pharmaceutics

journal homepage: www.elsevier.com/locate/ijpharm

Development of topical eye-drops of lactoferrin-loaded biodegradable nanoparticles for the treatment of anterior segment inflammatory processes

Ana López-Machado [a,b], Natalia Díaz [c,d,e], Amanda Cano [a,b,f], Marta Espina [a,b], Josefa Badía [c,d,e], Laura Baldomà [c,d,e], Ana Cristina Calpena [a,b], Martina Biancardi [g], Eliana B. Souto [h,i], María Luisa García [a,b,f,*,1], Elena Sánchez-López [a,b,d,*,1]

[a] Department of Pharmacy, Pharmaceutical Technology and Physical Chemistry, Faculty of Pharmacy and Food Sciences, University of Barcelona, Barcelona, Spain
[b] Institute of Nanoscience and Nanotechnology (IN2UB), University of Barcelona, Barcelona, Spain
[c] Department of Biochemistry & Physiology, Faculty of Pharmacy & Food Sciences, University of Barcelona, Barcelona, Spain
[d] Institute of Biomedicine, University of Barcelona (IBUB), Barcelona, Spain
[e] Institut de Recerca Sant Joan de Deu (IRSJD), Barcelona, Spain
[f] Biomedical Research Networking Centre in Neurodegenerative Diseases (CIBERNED), Madrid, Spain
[g] Technology Dedicated to Care, Barcelona, Spain
[h] Department of Pharmaceutical Technology, Faculty of Pharmacy, University of Coimbra, Portugal
[i] CEB—Centre of Biological Engineering, Campus de Gualtar, University of Minho, 4710-057 Braga, Portugal

ARTICLE INFO

Keywords:
Lactoferrin
Nanoparticles
PLGA
Ocular anti-inflammatory
Drug delivery
Cytotoxicity

ABSTRACT

Ocular inflammation is one of the most common comorbidities associated to ophthalmic surgeries and disorders. Since conventional topical ophthalmic treatments present disadvantages such as low bioavailability and relevant side effects, natural alternatives constitute an unmet medical need. In this sense, lactoferrin, a high molecular weight protein, is a promising alternative against inflammation. However, lactoferrin aqueous instability and high nasolacrimal duct drainage compromises its potential effectiveness. Moreover, nanotechnology has led to an improvement in the administration of active compounds with compromised biopharmaceutical profiles. Here, we incorporate lactoferrin into biodegradable polymeric nanoparticles and optimized the formulation using the design of experiments approach. A monodisperse nanoparticles population was obtained with an average size around 130 nm and positive surface charge. Pharmacokinetic and pharmacodynamic behaviour were improved by the nanoparticles showing a prolonged lactoferrin release profile. Lactoferrin nanoparticles were non-cytotoxic and non-irritant neither *in vitro* nor *in vivo*. Moreover, nanoparticles exhibited significantly increased anti-inflammatory efficacy in cell culture and preclinical assays. In conclusion, lactoferrin loaded nanoparticles constitute a safe and novel nanotechnological tool suitable for the treatment of ocular inflammation.

1. Introduction

Ocular inflammation constitutes one of the most common consequences associated to ophthalmic disorders and it is associated to a wide range of pathologies (Mazet et al., 2020). It is a non-specific response to an external insult that includes different molecular and functional mediators, involving recruitment and activation of inflammatory cells and release of inflammatory mediators, such as cytokines, interleukins, prostaglandins and enzymes (Anfuso et al., 2017).

Regarding the anterior segment of the eye, a wide range of ocular

Abbreviations: AFM, Atomic force microscopy; NSAIDs, Anti-inflammatory drugs; Z_{av}, Average particle size; bLF, Bovine LF; DSC, Differential scanning calorimetry; EE, Encapsulation efficiency; FTIR, Fourier transform infrared; GRAS, Generally recognized as safe substance; HCE-2, Human corneal epithelial cells; IL-8, Interleukin 8; P188, Kolliphor P188®; LF, Lactoferrin; LPS, Lipopolysaccharide; NPs, Nanoparticles; NF-κB, Nuclear transcription factor kappa B; PLGA, Poly (lactic-co-glycolic acid); PI, Polydispersity index; ROS, Reactive oxygen species; Rho, Rhodamine 110; SA, Sodium arachidonate; MTT, Tetrazolium bromide; TEM, Transmission electron microscopy; TFA, Trifluoroacetic acid; TNF-α, Tumour necrosis factor α; ZP, Zeta potential.

* Corresponding authors at: Department of Pharmacy, Pharmaceutical Technology and Physical Chemistry, Faculty of Pharmacy and Food Sciences, University of Barcelona, Barcelona, Spain.
E-mail addresses: marisagarcia@ub.edu (M.L. García), esanchezlopez@ub.edu (E. Sánchez-López).
[1] Both have equally contributed.

https://doi.org/10.1016/j.ijpharm.2021.121188
Received 23 June 2021; Received in revised form 30 September 2021; Accepted 11 October 2021
Available online 14 October 2021

pathologies are tightly associated with ocular inflammation including dry eye disease or keratoconjunctivitis *sicca* (Chen et al., 2019), microbial or viral infection (Pearlman et al., 2013), post-operative inflammation, seasonal allergic conjunctivitis, blepharitis (Tamhane et al., 2019), or uveitis related to patients with psoriatic arthritis (Abbouda et al., 2017; Foster et al., 2016).

In this area, topical administration is the most suitable route for ocular treatments due to its ease of handling, non-invasiveness, and effectiveness avoiding systemic side effects associated with oral administration (Mazet et al., 2020).

Current treatment for ocular inflammation consists mainly on the administration of corticosteroids and non-steroidal anti-inflammatory drugs (NSAIDs), in monotherapy or in combination. Nonetheless, its prolonged use include severe adverse events (Caplan et al., 2017; Carnahan and Goldstein, 2000; Foster et al., 2016).

To address these issues, the research for alternatives in the treatment of ocular inflammation is crucial. Therefore, recently, lactoferrin (LF) is an iron-binding glycoprotein that modulates the innate and adaptive reactions of the immunological system. This protein is associated to anti-inflammatory effects as well as antibacterial, antifungal, antiviral, antiparasitic and immunomodulatory properties. Moreover, it has been investigated due to its multifunctional capacities to combat several ocular diseases (González-chávez et al., 2009; Kanyshkova et al., 2001; Lee et al., 2020; Wang et al., 2017).

LF three-dimensional structure reveals a protein folded into two highly homologous lobes with iron-binding capacity. Each of these lobes can bind a ferric ion stably and reversibly, with the simultaneous binding of a bicarbonate anion. LF is secreted by neutrophils and exocrine glands. Colostrum and milk present the highest levels of this glycoprotein, but it is also detected in fluids such as tears, saliva, or gastrointestinal secretions (Tamhane et al., 2019). During infection or inflammation processes it has been observed that LF concentration increases due to neutrophil recruitment (Ward et al., 2005). Specifically, at ocular level, LF is one of the most abundant proteins in the tear fluid, comprising around 20–30 % in basal and reflex tears (Hanstock et al., 2019). Moreover, LF is presented in vitreous humour and different ocular tissues, such as cornea, iris and retinal pigment epithelium (Rageh et al., 2016).

Human and bovine LF possess similar functions due to their high sequence homology (Rosa et al., 2017). Therefore, most of the *in vitro* and *in vivo* studies have been carried out employing bovine LF (bLF), generally recognized as safe substance (GRAS) by the Food and Drug Administration (FDA) and the European Food Safety Authority (EFSA) (European Food Safety Authority, 2012; Rosa et al., 2017). bLF has a powerful anti-inflammatory activity (Håversen et al., 2002). It is internalized from the apical side of the host cells and located in the nucleus, being N-lobe the responsible for the union, internalization and orientation (Suzuki et al., 2009). Thus, it has the capacity of modulating the inflammatory response in corneal epithelial cells attenuating the nuclear transcription factor kappa B (NF-κB)-induced transcription of genes for various inflammatory mediators (Gu and Wu, 2016; Rosa et al., 2017).

In addition, the generation of reactive oxygen species (ROS) is also involved in the inflammation process. It has been described that free iron is responsible for potentiating redox reactions, as it can easily accept or donate electrons that contribute to the formation of ROS (Kanwar et al., 2015). Therefore, eliminating free iron and inhibiting redox activities through chelation is a potentially useful therapeutic strategy to treat inflammatory ocular diseases (Chen et al., 2017).

Nonetheless, bLF presents some instability in aqueous solution (Wang et al., 2019). In addition, hydrophilic substances administered as eye drops are rapidly eliminated via conjunctiva and nasolacrimal duct. It results in a pre-corneal drug half-life of 1–3 min and it has been reported that, due to tear turnover, only 5 % of the dose penetrates the cornea and reaches intraocular tissues (Liu et al., 2015; Sánchez-López et al., 2016).

During recent years, ocular active administration using controlled release systems has been emerging owing to improved permeability, bioavailability and stability, providing great advantages over conventional pharmaceutical dosage forms (Cano et al., 2017).

Therefore, to overcome these problems, drug encapsulation into biodegradable polymeric nanoparticles (NPs) has been carried out in order to increase its stability, therapeutic activity, and half-life in the ocular tissues allowing its release in a sustained way (Shi et al., 2010).

One of the most widely used polymers in these drug delivery systems is poly (lactic-co-glycolic acid) (PLGA), due to its biocompatibility and biodegradability. This compound is accepted by European Medicines Agency (EMA) and Food and Drug Administration (FDA) as Generally regarded as safe subtance (GRAS) that possess the ability of vectorization of the organism towards the therapeutic target (Sharma et al., 2016).

Hence, the aim of this study was the physicochemical development of polymeric bLF-NPs as topical ophthalmic drug delivery system for the treatment of ocular inflammation. This study highlights the incorporation of high molecular weight proteins like bLF within nanostructured systems. Moreover, the evaluation of their cytotoxicity and anti-inflammatory efficacy has been carried out by both *in vitro* and *in vivo* studies. Furthermore, corneal permeability and prolonged release of the active compound were decisive in the formulation assembly. Thus, the objective of improving the pharmacokinetic and pharmacodynamic drug profile was also pursued.

2. Experimental

2.1. Materials

bLF was purchased from Azienda Chimica e Farmaceutica (Italy); PLGA Resomer® 50:50 503H was acquired from Boehringer Ingelheim (Germany); ethyl acetate and Kolliphor®P188 (P188), ethyl-3-(3-dimethylaminopropyl) carbodiimide (EDC), N-hydroxysuccinimide (NHS), N-diisopropylethylamine (DIEA), rhodamine 110 (Rho) chloride, trypsin-EDTA (1X), insulin, hydrocortisone, lipopolysaccharide (LPS) and tetrazolium bromide (MTT) were purchased from Sigma Aldrich (MO, USA). Keratinocyte serum-free medium, human recombinant epidermal growth factor, bovine pituitary extract, penicillin, streptomycin, fetal bovine serum, IL-8 and TNF-α Human ELISA Kit were obtained from Thermo Fisher Scientific (Life Technologies, CA, USA). Human corneal epithelial cell line immortalized with adenovirus 12-SV40 hybrid virus (HCE-2, ATCC® CRL-11135) was purchased from LGC Standards (Barcelona, Spain). Water filtered through a Millipore® MilliQ system was used for all the experiments and all the other reagents used were of analytical grade.

2.2. Fabrication of nanoparticles

bLF loaded NPs were produced by a modified double emulsion method described elsewhere (Lamprecht et al., 2000; Tao Meng et al., 2003). Briefly, the organic phase (o) was formed dissolving a predetermined amount of PLGA in 2 mL of ethyl acetate. Aqueous phase (w_1) was obtained by dissolving bLF in 2.5 mL of deionized water. The primary emulsion (w_1/o) was formed by applying ultrasonic energy during 30 s. Secondary emulsion ($w_1/o/w_2$) was formed by mixing the w_1/o emulsion with 1.5 mL of deionized water containing P188 (1.8 $mg{\cdot}mL^{-1}$) following by the application of ultrasonic energy. Then, 1 mL of P188 (0.02 $mg{\cdot}mL^{-1}$) was added dropwise under magnetic stirring, and the organic solvent was evaporated overnight (Sánchez-López et al., 2018).

The production of NPs fluorescently labelled with rhodamine 110 (Rho) followed the same approach above described, but adding 20 % of Rho-PLGA from the total amount of PLGA (Gonzalez-Pizarro et al., 2019a; Iqbal et al., 2015). Briefly, for the obtention of polymer Rho-PLGA, a quantity of PLGA 503H reacted with NHS and EDC dissolved in chloroform. Subsequently, the activated PLGA (NHS-PLGA) was

subjected to a procedure of washing/precipitation three times with cold diethyl ether. The resultant NHS-PLGA was dried and labelled with Rho by dissolving in chloroform with DIEA. The obtained polymer was submitted to three washing/precipitation cycles by adding an 80/20 mixture of diethyl ether and cold methanol. Finally, it was lyophilized and stored at − 20 °C (Gonzalez-Pizarro et al., 2019a).

2.3. Design of experiments

To obtain the optimal formulation, a design of experiments (DoE) was employed using a 2^3 central composite design matrix generated by StatGraphics Centurion XVI.I. This design was developed to analyse the effects of the independents variables (bLF, PLGA and P188 concentrations) on the dependent parameters (average particle size (Z_{av}), polydispersity index (PI), zeta potential (ZP) and encapsulation efficiency (EE)) (Nekkanti et al., 2015). Each factor was studied at five different levels (see Table 1) and the responses were modelled through the full second-order polynomial Eqn 1:

$$Y=\beta_0+\beta_1X_1+\beta_2X_2+\beta_3X_3+\beta_{11}X_1^2+\beta_{22}X_2^2+\beta_{33}X_3^2+\beta_{12}X_1X_2+\beta_{13}X_1X_3+\beta_{23}X_2X_3 \quad (1)$$

where Y is the measured response, β_0 to β_{23} are the regression coefficients and X_1,X_2 and X_3 are the studied factors (Cano et al., 2018).

2.4. Physicochemical characterization

Different physicochemical parameters were determined to characterize the bLF-NPs using a ZetaSizer NanoZS (Malvern Instruments, Malvern, UK). Z_{av} and PI of NPs were determined by dynamic light scattering. ZP was determined measuring particle electrophoretic mobility using a combination of Laser doppler velocimetry and phase analysis light scattering (PALS). Samples were diluted (1:20) and measurements were carried out by triplicate in 10 mm diameter cells and disposable capillary cells DTS1070 (Malvern Instruments), respectively, at 25 °C (Anaraki et al., 2020).

2.5. Encapsulation efficiency

2.5.1. Indirect determination of encapsulation efficiency

With the objective of elucidating the percentage of bLF encapsulated in the NPs, the EE was determined indirectly by measuring the non-entrapped drug in the dispersion medium. The non-loaded drug was separated from NPs by ultracentrifugation at 4 °C and 45000 rpm for 60 min (Beckman Optima®, Ultracentrifuge, California, USA). Then, supernatant was used to evaluate the EE according to the following Eqn 2 (Gonzalez-Pizarro et al., 2018):

$$\text{EE } (\%) = \frac{\text{Total amount of bLF Free amount o fbLF}}{\text{Total amount of bLF}} \cdot 100 \quad (2)$$

The amount of the bLF in the aqueous phase was quantified by a reverse-phase high-performance liquid chromatography (RP-HPLC) method (Aguilar, 2004). The methodology used was validated in accordance with international guidelines (EMEA, 2011), including the evaluation of linearity, sensitivity, accuracy, and precision. Briefly, samples were quantified using HPLC Waters 2695 (Waters, Massachusetts, USA) separation module and a Europa® Protein 300 C_8 column (5 µm, 250 × 4.6 mm) with a mobile phase formed by a water phase of 0.1 % trifluoro acetic acid (TFA) and an organic phase of acetonitrile/water/TFA (95:5:0.1), in a gradient (from 95 % to 25 % of water phase in 4 min and back in next 4 min, maintaining this ratio until 25 min) at a flow rate of 0.75 mL·min^{-1}. A calibration curve with a bLF concentration ranges from 0.1 to 1 mg·mL^{-1} was prepared. A diode array detector Waters® 2996 at a wavelength of 219 nm was used to detect the bLF and data were processed using Empower 3® Software.

Table 1
Matrix of the factorial design including coded levels and their corresponding values in the experimental design.

	Levels				
Factor	−1.68	−1	0	+1	+1.68
cbLF (mg·mL^{-1})	1.60	5	10	15	18.40
cPLGA (mg·mL^{-1})	0.32	1	2	3	3.68
cP188 (mg·mL^{-1})	7.28	10	14	18	20.72

2.5.2. Direct determination of the encapsulation efficiency: Immunohistochemical method

Electrophoresis of bLF was carried out using the polyacrylamide gel in the presence of sodium dodecyl sulphate (SDS). This technique is used to separate and identify proteins based on their molecular weight. Proteins in the presence of SDS are denatured and negatively charged so they migrate to the anode in an electric field based on molecular weight. Gels with a polyacrylamide concentration of 10 % were used. The molecular weight marker used was the BENCHMARK® Prestained Protein Ladder (Invitrogen®). Subsequently, gel staining was performed with Coomassie bright blue, and protein analysis was carried out by Western Blot (Pillai-Kastoori et al., 2020). The protein present in the samples was detected using antibodies specific for bLF.

2.6. Morphological characterization

Morphology of the optimized formulation of bLF-NPs was determined by Transmission Electron Microscopy (TEM), performed on a JEM 1010 microscope (JEOL, Akishima, Japan). Copper grids were activated with UV light and diluted bLF-NPs (1:5) were placed on the grid surface, previously subjected to negative staining with uranyl acetate (2 %) (Cano et al., 2018).

Surface morphology and roughness were characterized by Atomic Force Microscopy (AFM) on a Dimension Icon microscope (Bruker, Massachusetts, USA). bLF-NPs were taped onto a glass slide and scanned in tapping mode (scan size of 2 µm, scan rate of 0.894 Hz, samples/line of 512) (You et al., 2020).

2.7. Interaction studies

bLF-NPs were ultracentrifuged (Beckman Optima® Ultracentrifuge, California, USA) at 45000 rpm and 4 °C, for 60 min, and the pellet was dried and pulverized to obtain the dry powder samples. Then, thermograms were obtained by Differential Scanning Calorimetry (DSC) on a Mettler T A 4000 system (Greifensee, Switzerland) equipped with a DSC-25 cell. Samples were weighed using a Mettler M3 Microbalance (Mettler Toledo, Ohio, USA), in perforated aluminium pans and heated under a flow nitrogen at a rate of 10 °C/min. Data were evaluated using 9.01 DB Metter STARe V software (Mettler Toledo, Ohio, USA) (Sánchez-López et al., 2016).

Fourier Transform Infrared (FTIR) spectra of bLF-NPs and their components were carried out using a Thermo Scientific Nicolet iZ10 with an ATR diamond and DGTS detector. The scanning range was 525–4000 cm^{-1}, the spectral resolution was 4 cm^{-1} and 32 scans (Carvajal-Vidal et al., 2019).

2.8. γ-Irradiation sterilization

With the aim of eliminating any source of bacterial contamination, bLF-NPs were sterilized using a dose of 25 kGy of ^{60}Co as γ-irradiation source (Aragogamma, Barcelona, Spain). According to the European Pharmacopoeia, this dose represents the adequate absorbed dose for the purpose of sterilizing pharmaceutical products when bioburden is not known (Bozdag et al., 2005), maintaining a valid sterility assurance level (SAL) of 10^{-6} (Ramos Yacasi et al., 2016). The influence of γ-irradiation on the physicochemical properties of the NPs was evaluated.

2.9. Biopharmaceutical behaviour

2.9.1. In vitro drug release

In vitro release profile was evaluated using a direct dialysis bag technique due to the water solubility of bLF (Cano et al., 2018). The release medium was 0.1 M phosphate buffer saline solution (PBS) at pH 7.4, and bLF-NPs were place in 1 mL dialysis bags (Float-A-Lyzer® dialysis device, 1000 kDa) (Repligen®, Massachusetts, USA). Dialysis medium was PBS buffer, and it was maintained under magnetic stirring at 37 ℃. At different time intervals, 1 mL of sample was taken from the release medium and replaced with fresh buffer solution. It was analysed by RP-HPLC method previously described and data were adjusted to the most common pharmacokinetic models (Cano et al., 2019).

2.9.2. Ex vivo corneal permeation study

The ex vivo bLF permeation study from bLF-NPs was carried out using isolated cornea from New Zealand rabbits (2.5–3.0 kg males), according to the Ethics Committee of Animals Experimentation from the University of Barcelona (CEEA-UB), and under veterinary supervision. Animals were anesthetized with intramuscular administration of ketamine HCl (35 $mg{\cdot}kg^{-1}$) and xylazine (5 $mg{\cdot}kg^{-1}$) and euthanized by an overdose of sodium pentobarbital (100 $mg{\cdot}kg^{-1}$) administered through marginal ear vein under deep anaesthesia (Sánchez-López et al., 2016). Eyes were removed, immediately excised, and transported in artificial tear solution to the laboratory. Corneas were fixed in Franz cells between the donor and receptor compartment with a diffusion area of 0.64 cm^2. In all experiments, 1 mL of the test formulation (bLF-NPs or 9.32 $mg{\cdot}mL^{-1}$ of free bLF) was incubated in the donor compartment and immediately covered to avoid the sample evaporation. The receptor compartment was filled with PBS at 32 ± 0.5 °C and it was kept under magnetic stirring. 300 µL were withdrawn from the receptor compartment at pre-selected times during 6 h and replaced by an equivalent volume of fresh receptor medium at the same temperature. Sink conditions were maintained throughout the experiment.

The cumulative amount of bLF permeated was calculated, at each time point, from bLF amount in receptor medium and plotted as function time (Gonzalez-Pizarro et al., 2018). Samples were measured using the RP-HPLC method (Smith et al., 1985; Wang et al., 2017).

To quantify the sample inside the tissue, recovery of the corneal structure was analysed. The tissue was washed with distilled water, weighted, and sonicated in MQ® water for an hour, using an ultrasound bath.

Values were reported as the mean ± SD. Three replicates of each sample were carried out. Permeation parameters were obtained by plotting the cumulative bLF permeated versus time, calculating x-intercept by linear regression analysis. The permeability coefficient (K_p) ($cm{\cdot}h^{-1}$), steady-state flux (J) ($\mu g{\cdot}h^{-1}{\cdot}cm^{-2}$) and amount of permeated at 24 h (Q24) (µg) were calculated (Gómez-Segura et al., 2020).

2.10. NP short-term stability

The stability of bLF-NPs stored at different temperatures (4 and 25 °C) was studied by multiple light scattering using Turbiscan® Lab (Iesmat, Madrid, Spain). This technique identifies the different destabilization phenomena of the colloidal suspension such as creaming, sedimentation, flocculation, and coalescence. For this purpose, a glass measurement cell was filled with 20 mL of sample. The light source is a pulsed near infrared light source (λ = 880 nm) and it is received by backscattering detector at an angle of 45° from the incident beam due to the opacity of the NPs formulation. Backscattering data were acquired at 1, 15 and 30 days for 24 h at intervals of 1 h. Moreover, morphometric parameters (Z_{av}, PI and ZP) were also measured.

2.11. Cell culture assays

2.11.1. Cytotoxicity assays

Human corneal epithelial cells (HCE-2) were used to perform cytotoxicity assays. As these cells belong to corneal tissue, they present a greatly suitable line to carry out the *in vitro* studies of bLF-NPs for ocular administration. Keratinocyte serum-free medium was the culture medium for HCE-2 cells. It was supplemented with bovine pituitary extract 0.05 $mg{\cdot}mL^{-1}$ and epidermal growth factor 5 $ng{\cdot}mL^{-1}$ containing insulin 0.005 $mg{\cdot}mL^{-1}$, 10 % (v/v), fetal bovine serum, hydrocortisone 500 $ng{\cdot}mL^{-1}$ and penicillin 100 $U{\cdot}mL^{-1}$ plus streptomycin 100 $mg{\cdot}mL^{-1}$. Cells were grown on a culture flask to 80 % confluency in a humidified 10 % CO_2 atmosphere at 37 °C.

To highlight the possible cytotoxicity of the formulations, cell viability tests were performed on HCE-2 corneal cell line using MTT (Bromide of 3-(4,5-dimethyl-2-thiazoyl)-2,5-diphenyltetrazole as an indicator of viability. 0.1 mL of a cell density of 1×10^5 were seeded in 96-well plates and incubated at 37 °C for 24 h. Later, cells were exposed to bLF-NPs and free bLF at different drug concentrations (0.04–0.1 $mg{\cdot}mL^{-1}$). After 24 h of incubation, cells were washed with PBS and incubated with 0.25 % MTT in fresh medium for 2 h. Then, this medium was extracted, and DMSO was added for cell lysis. The absorbance was measured at λ = 560 nm by an automatic Modulus™ Microplate Photometer (Turner BioSystems, CA, USA). Data were analysed by calculating the percentage of MTT reduction and expressed as percentage of control (untreated cells).

2.11.2. Determination of proinflammatory cytokines

To evaluate the anti-inflammatory activity of the bLF-NPs and free bLF, HCE-2 cells were seeded (1×10^5 $cell{\cdot}mL^{-1}$) in 12-well plates and grown until 90 % confluency. Samples were added to the culture medium at 0.2 $mg{\cdot}mL^{-1}$ (drug concentration of loaded NPs) and inflammation was induced with lipopolysaccharide (LPS) (1 $\mu g{\cdot}mL^{-1}$). Cells stimulated only with LPS were used as a positive control and untreated cells as a negative control. After 24 h incubation, the supernatants were collected and centrifuged (16000 g for 10 min) at 4 °C and stored at –80 °C until use. Unknown levels of the pro-inflammatory cytokines, interleukin 8 (IL-8) and tumour necrosis factor α (TNF-α), were quantified using ELISA kits (BD Biosciences, CA, USA) according to manufacturer's instructions. Results were expressed as $pg{\cdot}mL^{-1}$.

2.11.3. Cellular uptake assay

To evaluate the internalization of NPs in HCE-2 cells, 1×10^5 $cell{\cdot}mL^{-1}$ HCE-2 were grown in eight-well chamber slider (ibidi®, Gräfelfing, Germany) until 80 % confluence and posteriorly incubated with bLF-NPs at different dilutions ratios (1:10; 1:50 and 1:100) at 37 °C for 48 h. Non-internalized NPs were removed by washing three times with PBS and cells were fixed with 3 % paraformaldehyde for 30 min at 25 °C. Subsequently, cells were subjected to triple PBS washes and then, the nuclei were stained with 4′,6-diamidino-2-phenylindole (DAPI) for 15 min at 25 °C. Finally, mounting solution (PBS) was added for microscopic analysis. Images were acquired using a Leica TCS SP5 confocal laser scanning microscopy (Leica Microsystems, Wetzlar, Germany) with a 63x oil immersion objective lens (Gonzalez-Pizarro et al., 2019a).

2.12. Ocular tolerance

2.12.1. In vitro study: HET CAM test

In vitro ocular tolerance was assessed using the HET-CAM test to ensure that the formulation of bLF-NPs was non-irritating when administered as eye-drops. Irritation, coagulation, and haemorrhage phenomena were measured by applying 300 µL of the formulation

studied on chorioallantoic membrane of a fertilized chicken egg and monitoring it during the first 5 min after the application.

This assay was conducted according to the guidelines of ICCVAM (The Interagency Coordinating Committee on the Validation of Alternative Methods). The development of the test was carried out using 3 eggs for each group (free bLF, bLF-NPs, positive control (NaOH 0.1 M) and negative control (0.9 % NaCl)). The ocular irritation index (OII) was calculated by the sum of the scores of each injury according to the following expression (Eqn 3):

$$OII = \frac{(301 - H)\cdot 5}{300} + \frac{(301 - V)\cdot 7}{300} + \frac{(301 - C)\cdot 9}{300} \quad (3)$$

where H, V and C are times (s) until the start of haemorrhage (H), vasoconstriction (V) and coagulation (C), respectively. The formulations were classified according to the following: OII $\leq$ 0.9 non-irritating; 0.9 $<$ OII $\leq$ 4.9 weakly irritating; 4.9 $<$ OII $\leq$ 8.9 moderately irritating; 8.9 $<$ OII $\leq$ 21 irritating (Derouiche and Abdennour, 2017; Shalom et al., 2017).

2.12.2. In vivo study: Draize test

The formulations were evaluated using primary eye irritation test of Draize to ensure the results obtained from the HEM-CAM test (Sánchez-López et al., 2016). For this experiment, New Zealand male albino rabbits (2.0–2.5 kg, St. Feliu de Codines, Barcelona, Spain) were used. 50 μL of each sample were instilled in the ocular conjunctival sac (n = 3/group) and a mild massage was applied to guarantee the passage of the sample through the eyeball. The possible appearance of irritation signs (corneal opacity and area of corneal involvement, conjunctival hyperemia, chemosis, ocular discharges, and iris abnormalities) was observed at the time of instillation and after 1 h from its application and if necessary, at predefined intervals: 24 h, 48 h, 72 h, 7 days, and 21 days after administration. The opposite untreated eye was used as a negative control. Draize test score was determined directly by observing the anterior segment of the eye and changes in the structures of the cornea (turbidity or opacity), iris and conjunctiva (congestion, chemosis, swelling and secretion).

2.13. In vivo efficacy studies

2.13.1. Prevention of inflammation

The evaluation of the prevention of inflammation ability of bLF-NPs in comparison with the free bLF and the control group (NaCl 0.9 %) was carried out. First, each sample was administered and subsequently, an inflammatory stimulus was applied in New Zealand male albino rabbits (n = 3/group). The study consisted of the application of 50 μL of each formulation. After 30 min of exposure, 50 μL of 0.5 % sodium arachidonate (SA) dissolved in PBS was instilled in the right eye and the left eye was used as a control. The evaluation of prevention of inflammation was carried out from the application of formulations up to 210 min, according to the Draize modified test scoring system (Sánchez-López et al., 2016).

2.13.2. Inflammation treatment

The induction of inflammation with the objective of evaluating the anti-inflammatory effect of bLF-NPs compared to the free protein and the control group (NaCl 0.9 %), was carried out using New Zealand male albino rabbits (n = 3/group). The study was conducted with the application of 50 μL of 0.5 % sodium arachidonate (SA) dissolved in PBS in the right eye, using the left eye as a control. After 30 min of exposure, 50 μL of each formulation was instilled. Evaluation of inflammation was performed from the application of formulations up to 180 min according to Draize modified scoring system (Sánchez-López et al., 2016).

2.14. Statistical analysis

Two-way ANOVA, followed by Tukey *post hoc* test, was performed for multi-group comparison. Student's *t* test was used for two-group comparisons. All the data are presented as the mean ± S.D. Statistical significance was set at $P < 0.05$ by using GraphPad Prism 8.4.3 and ImageJ was used to analyse images.

3. Results and discussion

3.1. Design of experiments

A composite central factorial design was carried out with the objective of optimizing the formulation, evaluating the effect of the concentrations of bLF, PLGA and P188 on the physicochemical properties of the developed NPs. The response parameters and their magnitudes for each of the 16 experiments are given in Table 2.

The response surface (Fig. 1a) and the Pareto diagram (Fig. 1b) showed that bLF concentration influences the EE, increasing the encapsulation of bLF at middle concentrations. At bLF concentrations between 8 and 11 $mg{\cdot}mL^{-1}$, an increase in EE was observed, reaching the 50–60 % encapsulation. Accordingly, the Pareto diagram (Fig. 1b) confirmed that only the bLF concentration exerted a significant influence on EE. With concentrations lower than 7 $mg{\cdot}mL^{-1}$, and higher than 12 $mg{\cdot}mL^{-1}$, EE markedly decreases. With regard to PLGA, although its influence is not statistically significant, from the surface responses plots, it can be observed that until reaching concentration values around 19 $mg{\cdot}mL^{-1}$, a directly proportional relationship between PLGA and EE is observed (at fixed P188 concentration of 1.8 $mg{\cdot}mL^{-1}$, and a bLF concentration around 9 $mg{\cdot}mL^{-1}$). However, after exceeding this concentration the EE begins to decrease. This trend may be explained by the limited polymer incorporation capacity and the bLF high molecular weight (87 kDa). Thus, meaning that at 19.01 $mg{\cdot}mL^{-1}$ the maximum loading capacity is reached.

Regarding the average size of the NPs, the response surface (Fig. 1c) reveals that at a constant concentration of PLGA (19.01 $mg{\cdot}mL^{-1}$), an intermediate concentration of bLF and low concentrations of surfactant favour lower particle sizes. In all cases, the NPs obtained have an average size bellow 250 nm, so they are all suitable for ocular administration (Wadhwa et al., 2009).

Likewise, the response surface (Fig. 1d) analysing the PI, shows that the surfactant concentration affects the values obtained significantly, observing that at higher concentrations of P188 and PLGA, the PI reaches values of 0.2 in the range of monomodal systems. Instead, at lower P188 concentrations optimal values of PI was obtained ($<$0.1), characteristic of a monodispersed system. This tendency can be explained by the phenomenon of absorption in the polymeric surface of the substances, given the positive charge that bLF-NPs possess. It is possible that bLF is being placed both inside the polymer matrix and on its surface. The surfactant is also placed on the NPs surface. Increasing the surfactant concentration, the surface of the NPs would be saturated, thus increasing the PI and their average size (Masoudipour et al., 2017). Yan et al. observed that the surface absorption of the surfactant can change the smooth polymeric NPs appearance into a slightly rough one (Yan et al., 2010).

The PLGA used possess a great negative ZP, due to the ionization on the surface of polymer of carboxylic end groups. However, it has been reported that the presence of surfactant P188 can lead to a reduction in their surface charge (Vega et al., 2012). The hydrophobic polyoxypropylene chains bind the surface of the NP, and the hydrophilic polyoxypropylene chains remain protruding in the medium around it, masking the negative surface charge present in the NPs. In this case, besides the surfactant, the active principle to be encapsulated, bLF, has a positive charge at medium pH, so it also covers the negative charge of the polymer, obtaining as a result a ZP of approximately + 30 mV. The positive charge prolongs the residence time on the epithelial layer of the cornea and thus facilitates drug penetration and achieves a sustained release (Andrés-Guerrero et al., 2017).

From the results obtained in the factorial design, an optimized

Table 2
Values of the 2^{3+} star central composite rotatable factorial design, parameters, and measured responses.

	cbLF		cP188		cPLGA		Z_{av}	PI	EE
	Coded level	(mg·mL^{-1})	Coded level	(mg·mL^{-1})	Coded level	(mg·mL^{-1})	(nm)		(%)
Factorial points									
1	−1	5	−1	1	−1	10	135.1 ± 2.5	0.122 ± 0.044	43.96
2	1	15	−1	1	−1	10	130.6 ± 1.9	0.138 ± 0.034	32.39
3	−1	5	1	3	−1	10	112.0 ± 3.2	0.090 ± 0.021	34.67
4	1	15	1	3	−1	10	110.2 ± 2.8	0.089 ± 0.031	23.26
5	−1	5	−1	1	1	18	133.1 ± 4.5	0.077 ± 0.002	44.83
6	1	15	−1	1	1	18	116.7 ± 1.6	0.074 ± 0.022	30.23
7	−1	5	1	3	1	18	187.0 ± 4.2	0.141 ± 0.010	49.36
8	1	15	1	3	1	18	146.5 ± 1.3	0.125 ± 0.021	44.83
Axial points									
9	1.68	1.6	0	2	0	14	134.7 ± 2.7	0.220 ± 0.024	35.18
10	−1.68	18.4	0	2	0	14	243.1 ± 7.6	0.083 ± 0.009	45.56
11	0	10	1.68	3.68	0	14	148.6 ± 1.2	0.143 ± 0.046	50.75
12	0	10	−1.68	0.32	0	14	157.4 ± 1.6	0.122 ± 0.028	47.87
13	0	10	0	2	1.68	20.72	148.2 ± 4.1	0.181 ± 0.012	37.94
14	0	10	0	2	−1.68	7.28	125.1 ± 1.3	0.144 ± 0.005	49.03
Center points									
15	0	10	0	2	0	14	146.0 ± 5.1	0.100 ± 0.027	55.82
16	0	10	0	2	0	14	132.2 ± 3.7	0.158 ± 0.019	50.60

Results presented as mean ± standard deviation.

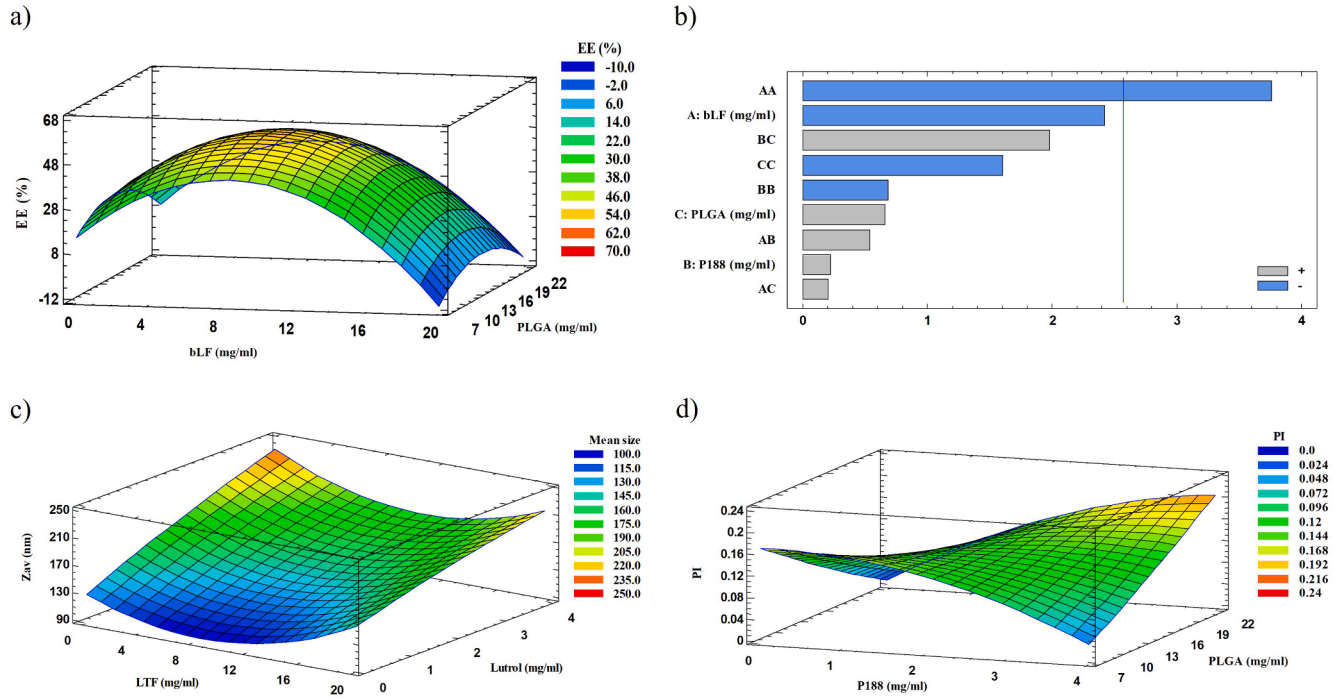

Fig. 1. (a) EE (%) surface response at a fixed P188 concentration (1.8 mg·mL^{-1}); (b) Pareto diagram for EE (%); (c) Z_{av} surface response at a fixed PLGA concentration (19.01 mg·mL^{-1}); (d) PI surface response at a fixed bLF concentration (9.32 mg·mL^{-1}).

Table 3
Physicochemical parameters of optimized bLF-NPs formulation.

cbLF (mg·mL^{-1})	cP188 (mg·mL^{-1})	cPLGA (mg·mL^{-1})	Z_{av} (nm)	PI	ZP (mV)	EE (%)
9.32	1.80	19.01	128.4 ± 5.0	0.058 ± 0.030	31.0 ± 0.8	56.00 ± 3.00

Data presented as mean ± standard deviation.

formulation was selected focusing mainly on the EE values (%) and on the adequate homogeneity of the sample (PI). It can be noted in Table 3, the optimized bLF concentration was 9.32 mg·mL^{-1}, 19.01 mg·mL^{-1} of polymer and 1.80 mg·mL^{-1} in the case of P188. The morphometry (Z_{av}, PI) and surface charge (ZP) of optimized formulation, determined by photon correlation spectroscopy and laser doppler velocimetry, respectively (Table 3) are suitable for ocular administration (Sánchez-López et al., 2016). The EE of bLF in the nanoparticles was 56.00 ± 3.00 %.

The NPs were ultracentrifuged, and the pellet and supernatant were separated. A polyacrylamide gel electrophoresis was carried out in

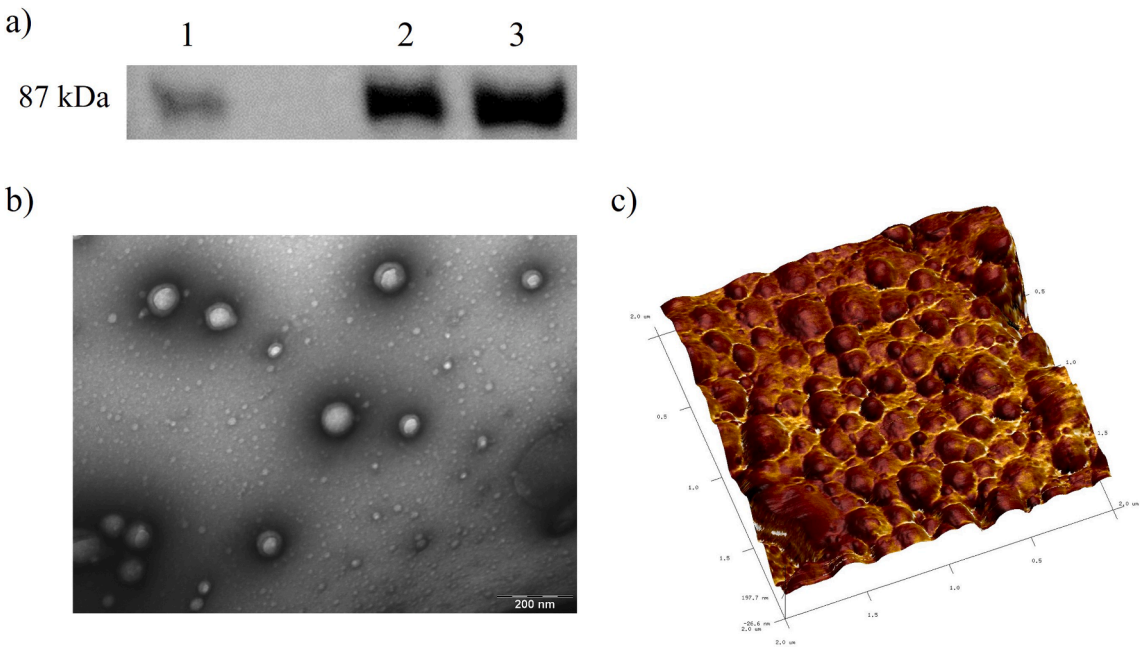

Fig 2. (a) bLF western blot analysis: 1. bLF control; 2. bLF in NPs; and 3. bLF in supernatant. (b) Microscopy studies of bLF-NPs by TEM; and (c) by AFM.

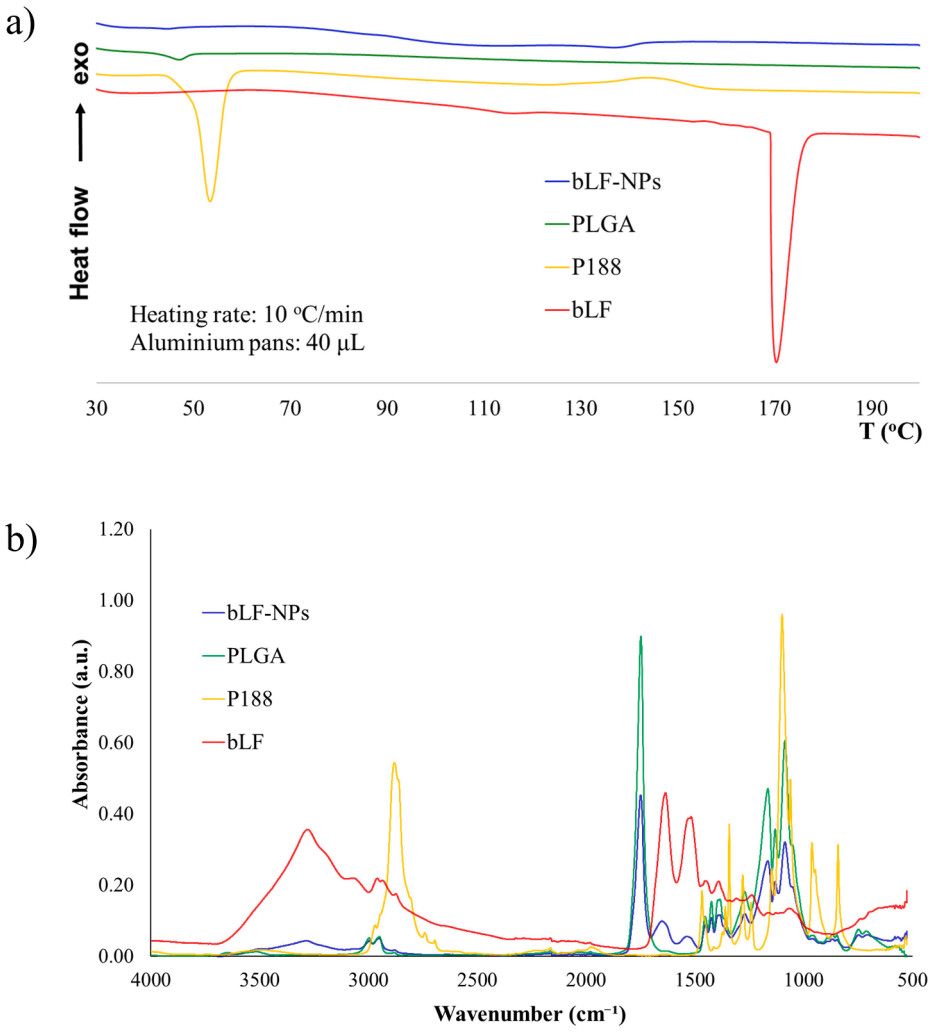

Fig. 3. Interaction studies of bLF-NPs. (a) DSC thermograms. (b) FTIR spectra.

denaturing conditions to separate the protein based on its molecular weight, then a western blot was carried out using anti-bLF antibodies. It was observed that 50 % of the initial bLF is within the systems thus confirming the results of EE (%) obtained by the HPLC method (Fig. 2a).

3.2. Morphological characterization

The morphological characterization of the optimized formulation of bLF-NPs was carried out by imaging using TEM and AFM (Fig. 2b and 2c). Images revealed a spherical shape of NPs, without any signs of aggregation phenomena and average particle diameters like those obtained in the morphometry tests performed by PCS.

3.3. Interaction studies

A factor that greatly affects the release of the active substance in *in vitro* and *in vivo* studies is the physical state of the drug inside the NPs. Therefore, a DSC study was carried out presenting the thermograms of bLF, P188, PLGA and bLF-NPs in the Fig. 3a. The bLF thermogram shows an acute endothermic accident that corresponds to its fusion, with a maximum temperature (T_{max}) of 170.41 °C which was not detected in bLF-NPs. This data suggest that bLF is encapsulated within the polymer matrix in an molecular dispersion or a solid solution state (Cano et al., 2019; Vega et al., 2012). P188 surfactant revealed a sharp melting endotherm characterized by a $\Delta H = 132.69\ J{\cdot}g^{-1}$ and a $T_{max} = 53.46$ °C (Gonzalez-Pizarro et al., 2018). It is noted a peak belonging PLGA that shows the onset of the glass transition (T_g) at 47.09 °C and in the bLF-NPs at 44.55 °C. This slight decrease of NPs T_g is attributed to the interaction between bLF and the polymer matrix (Sánchez-López et al., 2017).

To evaluate the interaction between bLF and PLGA, the FTIR analysis was performed (Fig. 3b). There was no evidence of covalent bonds between the protein and PLGA. The IR spectrum of bLF showed protein characteristic peaks, amide I at 1638 cm^{-1} due to C = O and C–N stretching vibration and amide II at 1520 cm^{-1} corresponding to the N–H bending with contribution of C–N stretching vibration. At 3279 cm^{-1} the band is given by the signal of the stretching vibration of O–H in water molecules, indicating the presence of residual H_2O (Wang et al., 2017; Yao et al., 2014). In the PLGA analysis, a characteristic strong band appeared at 1750 cm^{-1} due to stretching vibration of the carbonyl group. The weak peaks at 3002 and 2956 cm^{-1} correspond to stretching vibration of the alkanes and it appeared the medium peaks at the band of 1159 and 1088 cm^{-1} corresponding to the stretching vibration C–O and C–O–O, respectively (Gonzalez-Pizarro et al., 2018). In the case of P188 two strong peaks are showed, at 2874 cm^{-1} corresponding to the stretching vibration of CH and at 1096 cm^{-1} signal given by the stretching vibration of C–O (Yan et al., 2010). bLF-NPs showed a similar profile to PLGA and P188 with further weak intensity peaks due to bLF (amide I, II and O–H).

3.4. Effects of γ-irradiation on bLF-NPs

Since bLF-NPs were going to be administered as eye-drops, the formulation should be sterilized. In this sense, bLF-NPs were γ-irradiated and morphometrically characterized to ensure that the irradiation process did not affect the chemical structure of the system. As seen in Table 4, the results obtained demonstrated that γ-irradiation had no effect on the physicochemical parameters of the optimized NPs. It has shown not significant differences between NPs before and after sterilization. In this area, some authors reported that higher doses of γ-irradiation might favour the tendency to decrease particle size and ZP and increase the PI value of polymeric NPs. The difference in the case of bLF-NPs could be due to the use of a different surfactant that does not present the "long chain extension" phenomenon that leads to the chain scission, such as polyvinyl alcohol molecule, and a consequent reduction in NP molecular weight. However, these physicochemical changes generate a barely perceptible effect on the PLGA NPs. therefore, these slight modifications do not affect the medical properties of bLF-NPs (Ramos Yacasi et al., 2016; Tapia-Guerrero et al., 2020).

Table 4
Physicochemical properties and EE of bLF-NPs before and after sterilitzation.

	Average size (nm)	PI	ZP (mV)	EE (%)
bLF-NPs	131.6 ± 0.8	0.061 ± 0.019	30.4 ± 0.2	60.00 ± 3.00
bLF-NPs 25 kGy	134.7 ± 0.8	0.084 ± 0.020	28.5 ± 0.2	57.00 ± 1.00

Data presented as mean ± standard deviation.

3.5. Biopharmaceutical behaviour

3.5.1. In vitro drug release

The *in vitro* release of bLF from bLF-NPs and free bLF was carried out using a direct dialysis bag technique. The cumulative drug release profile revealed a controlled and prolonged release of bLF from NPs. Fig. 4a shows a faster release of the bLF from the NP during the first 5 h than free bLF, due to the drug weakly bound on the surface of NPs (Carvajal-Vidal et al., 2019). After that, the release speed decreases significantly, performing a sustained release without reaching a plateau (83.6 % after 48 h). PLGA matrix of controlled release systems usually presents an initial burst with a zero-order release profile and a posterior slower release from the polymeric matrix by diverse routes as diffusion through the polymer, erosion of the PLGA matrix or a combination of both (Cano et al., 2018; Fu and Kao, 2010; Sánchez-López et al., 2016). The Korsmeyer-Peppas model was the best one that adjusted the NPs formulation ($r^2 = 0.99$, AIC = 57.37). Free bLF showed a faster release, reaching 95 % after 22 h. The most appropriate release profile corresponds to a first-order equation ($r^2 = 0.97$, AIC = 80.76), characterized by a rapid release followed by a constant release (Fangueiro et al., 2016). To obtain the kinetic model that better fits for bLF release, data were adjusted to the most common kinetic models (Table 5).

3.5.2. Ex vivo corneal permeation

Ex vivo corneal permeation of bLF-NPs and free bLF were carried out to study its behaviour and compare different permeation parameters (Fig. 4b). According to Table 6, the bLF-NPs formulation presents statistically significant differences ($p < 0.05$) against free bLF in all examined permeation parameters, except for the case of bLF retained amount (QR). With respect to the steady-state flux (J) value is one third higher in the case of bLF-NPs, hence bLF from NPs permeated the cornea faster than free bLF. This fact is due to the greater lipophilicity of polymer than free protein, since the epithelium layer of the cornea is composed of lipid, and restricts the entry of hydrophilic substances, acting as a rate limiting factor for the eye level drug administration (Soni et al., 2019; Talluri et al., 2010). The different permeation parameters follow the same ratio, with the permeability coefficient (K_p) and the quantity permeated at 24 h (Q24) higher in the case of bLF-NPs than in the free bLF. It justifies the effect of bLF on the cornea and aqueous humor (Sánchez-López et al., 2016). Otherwise, no significant differences in the bLF QR in both formulations can be observed. Regarding the NPs formulation, the retained quantity may be from the non-encapsulated percentage of bLF and the initial burst from the fraction of bLF weakly bound or adsorbed on the surface area of the NPs (Vega et al., 2012).

Therefore, this formulation may deliver the drug effectively to the specified area by releasing bLF slowly across the corneal tissue, which would be beneficial for the treatment of ocular inflammation such as that induced by allergens, traumatisms or microbial infection (Schultz, 2018).

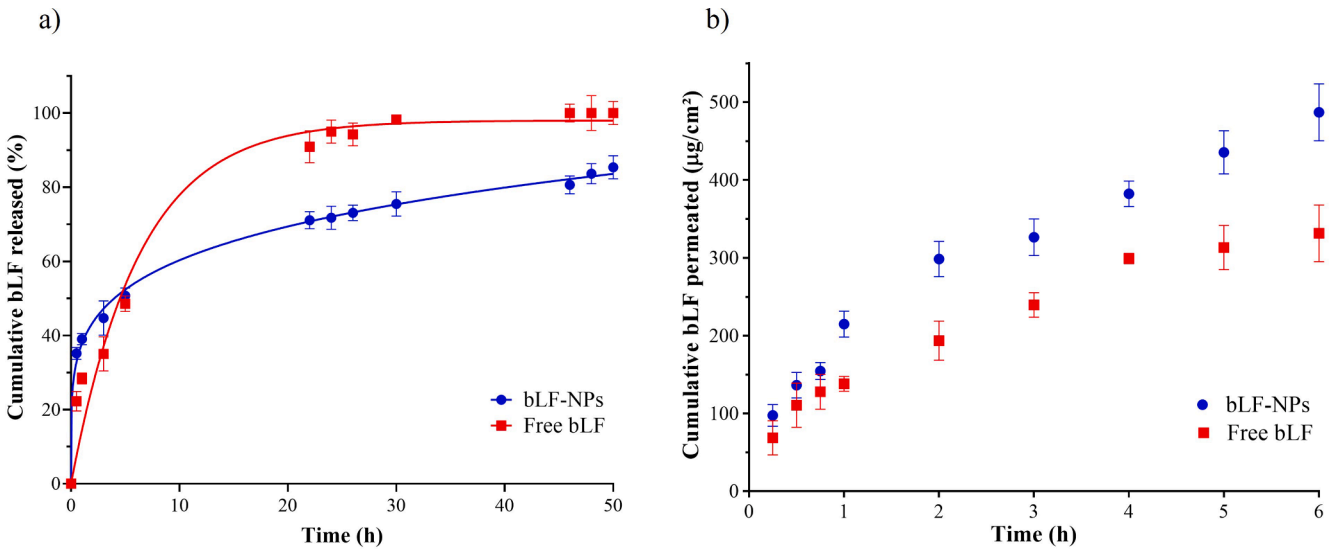

Fig. 4. (a) *In vitro* release profile of bLF-NPs (Korsmeyer-Peppas equation) against free bLF (first order equation). (b) *Ex vivo* corneal permeation profile of bLF-NPs compared with free bLF.

Table 5
Parameters for kinetic models of bLF-NPs and free drug solution.

Models	bLF-NPs		Free bLF	
	AIC	R^2	AIC	R^2
Zero Order	94.45	0.75	100.99	0.79
First Order	89.67	0.84	80.76	0.97
Higuchi	85.44	0.89	88.21	0.93
Hyperbola	82.79	0.91	77.88	0.97
Korsmeyer-Peppas	n = 0.007		n = 0.022	
	57.37	0.99	80.64	0.97

Table 6
Pharmacokinetic parameters adjusted to linear regression of the *ex vivo* corneal permeation of bLF-NPs against bLF.

Parameters	Free bLF	bLF-NPs
J ($\mu g \cdot h^{-1} \cdot cm^{-2}$)	70.55 ± 8.53	100.69 ± 16.75*
Kp · 10^3 ($cm \cdot h^{-1}$)	7.57 ± 0.91	10.80 ± 1.79*
Q24 (μg)	1081.63 ± 130.77	1544 ± 257.31*
QR ($\mu g \cdot g^{-1} \cdot cm^{-2}$)	1.07 ± 0.01	1.04 ± 0.01

Statistical significance: *$p < 0.05$. J, steady-state flux; Kp, permeability coefficient; Q24, permeated amount at 24 h; QR, retained amount.

3.6. Stability of nanoparticles

The prediction of the accelerated stability of the bLF-NPs was studied for 30 days. The optimized formulation was evaluated after 1, 15 and 30 days of storage at 4 and 25 °C. Turbiscan® Lab was used to determine destabilization processes such as the variation in the speed of migration of the particles (vertical sections of the graph) and the variation in size (horizontal section of the graph) (Fig. 5).

The migration of the particles to the upper part of the cell leads to a decrease in the concentration in the lower part. This is shown as a decrease in the backscatter signal (negative peak) and vice versa for the phenomena that occurs in the upper part of the vial. The backscatter profile with a deviation of ± 5 % is considered that it does not present significant variations in particle size. Variations of ± 10 % indicate that the formulation is unstable (Cano et al., 2017). This system allows predicting the instability processes of NPs before they can be detected by other techniques (Celia et al., 2009). It was observed that the backscattered light profile did not show fluctuations greater than 5 %, which indicates that the sample remained stable stored at 4 °C. The stability is associated with the high ZP of the NPs, approximately + 30 mV, avoiding electrostatic interaction between particles and its flocculation and precipitation (Retamal Marín et al., 2017).

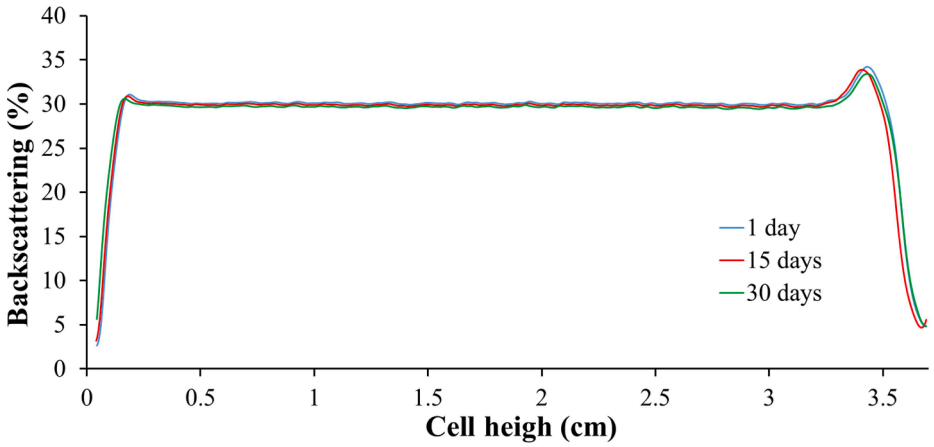

Fig. 5. Backscattering profile of bLF-NPs stored at 4 °C.

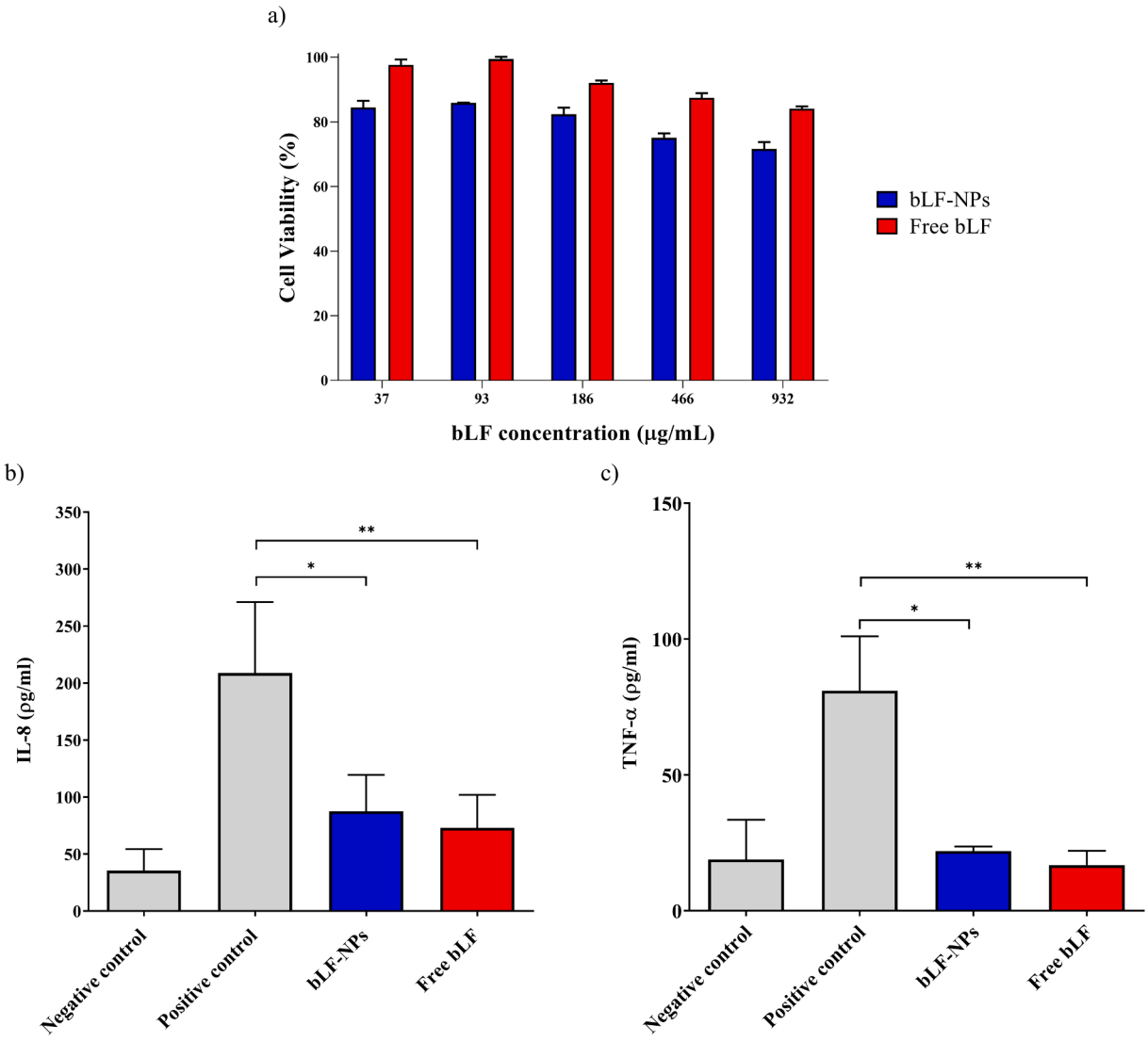

Fig. 6. (a) Effect of bLF-NPs on the viability of HCE-2 cells. The 100 % cell viability correspond with the average of MTT reduction values of untreated cells. (b) Quantification of secreted IL-8 proinflammatory cytokine in LPS-stimulated HCE-2 cells; (c) Quantification of secreted TNF-α. Negative control: no treatment; Positive control: LPS. Values are expressed as the mean ± SD; *$p < 0.05$; **$p < 0.01$ significantly lower than LPS-induced cytokine concentration.

3.7. Cytotoxicity of nanoparticles

Safety of bLF-NPs was assessed in HCE-2 cells. Results are shown in Fig. 6a. After 24 h of incubation, bLF-NPs did not show relevant cytotoxic effects. For concentrations up to 186 $\mu g \cdot mL^{-1}$, cell viability was higher than 80 %. At higher concentrations cell viability was close to 80 %. Free bLF showed no cytotoxic effects at all concentrations tested, since viability was kept close to 100 %.

LF is one of the most abundant components in the healthy tear fluid and contributes to iron retention mechanisms against pathogens and mitigates oxidative stress (Seen and Tong, 2018). Tear LF represents 20–30 % of the total proteins with concentrations ranging between 0.63 and 2.9 $mg \cdot mL^{-1}$, depending on sex and age, in healthy patients (Flanagan and Willcox, 2009; Lawrenson, 2018). Upon stimulation, such as oxidative stress or acute inflammation, the basal tear flow (1 $\mu L \cdot min^{-1}$) is significantly increased (Hanstock et al., 2019). bLF-NPs could provide a long-lasting protein concentration since the formulation is 3-fold more concentrated in lactoferrin than healthy tears. This fact improves its bioavailability, for cases in which the tears LF concentration is compromised (Ponzini et al., 2020).

Considering other formulation components, it has been reported that PLGA is a biocompatible, biodegradable, and safe polymer for the internalization and delivery of substances with pharmacological activities (Han et al., 2016).

Finally, the slight decrease in HCE cell viability, not observed for free bLF, may be due to the presence of the P188 surfactant. However, surfactants have been widely used as emulsifiers to prevent protein aggregation during manufacturing processes, shipping or storage (Wang et al., 2019; Yan et al., 2010). Although the most commonly used surfactants in biological products are polysorbates due to their widely known degradation, the evaluation of alternatives such as P188 has provided promising results. In fact, P188 is the surfactant that has been used in the production of commercialized biological drug products (Wang et al., 2019).

These results confirm the biocompatibility of the developed bLF-NPs with corneal cells, according to the generally recognized as safe (GRAS) designation of the formulation components (Han et al., 2016).

3.8. Anti-inflammatory activity of nanoparticles in HCE-2 cells

The ability of NPs to inhibit the inflammatory response produced by LPS was evaluated in HCE-2 cells through the analysis of IL-8 and TNF-α secreted cytokines (Fig. 6b and 6c). In the absence of NPs (positive control) LPS induced high secretion levels of both cytokines (Diaz-

Garrido et al., 2019). Treatment with bLF-NPs significantly decreased the expression of both cytokines to levels similar to that triggered by free bLF ($p < 0.05$).

There is evidence that in many ocular disorders involving chronic inflammation, tears present depleted levels of some proteins such as LF or lysozyme (Tamhane et al., 2019). In turn, these pathologies involve overexpression of different inflammatory mediators, specially IL-8 and TNF-α cytokines (Chen et al., 2019). It has been reported that elevated tear levels of IL-8 cause migration of neutrophils, basophils, and T lymphocytes causing exacerbation of the symptoms (Tamhane et al., 2019). Multiple studies have shown the presence of elevated levels of TNF-α, which is thought to represent a measure of the general inflammatory state of the ocular surface in patients with different ophthalmopathies (Aketa et al., 2017; Chen et al., 2019; Ghasemi, 2018).

LF has been reported to modulate the expression of several cytokines through different mechanisms (Lee et al., 2020). This protein is known to interact with cell surface receptors involved in the inflammatory response. For example, LF competes with bacterial LPS for binding to CD14 receptor, thus diminishing NF-κB-induced transcription of various genes for inflammatory mediators (Håversen et al., 2002; Kruzel et al., 2017). Meanwhile, in the context of iron sequestration, LF can control oxidative burst from neutrophils and macrophages that trigger the inflammatory response (Rosa et al., 2017). These results indicated that an anti-inflammatory effect was achieved with the bLF-NPs.

3.9. Cellular uptake of Rho-bLF-NPs

After 48 h incubation of HCE-2 cells with Rho-bLF-NPs at different concentrations (1:10; 1:50 and 1:100), the NP associated green fluorescence was visualized by confocal fluorescence microscopy. The nucleus was stained with DAPI. In the merged images, the Rho-NPs were found in the cytoplasm. As expected, untreated control cells did not show any green fluorescence signal from rhodamine, but nuclei were properly dyed with DAPI emitting blue florescent light (Fig. 7).

Different studies have proved the cellular internalization of PLGA NPs within corneal cells (Gonzalez-Pizarro et al., 2019a; Li et al., 2021; Sah et al., 2017; Sánchez-López et al., 2016). The uptake is dependent on the NPs size, concentration, and incubation time. It is showed that 100 nm NPs are internalized mainly by receptor-mediated endocytosis in corneal cells, rather than larger NPs that present absorption on the cell surface (Qaddoumi et al., 2004). Furthermore, the low density lipoprotein receptor-related protein 1 (LRP1) has been identified by Higuchi et al. as the primary LF receptor in corneal epithelium (Higuchi et al., 2016). The LRP1 expression levels were 8.7-fold higher than intelectin-1, another LF corneal receptor (Higuchi et al., 2016). This fact suggested that the bLF-NPs uptake may also be carried out through LRP1 pathway.

3.10. Ocular tolerance results

3.10.1. In vitro ocular tolerance of NPs

To stablish ocular tolerance, HET-CAM *in vitro* test was applied. bLF-NPs and free bLF were tested in the CAM of 3 eggs for formulation, to determine the possible rapid irritation reaction. The addition of 1 M NaOH (positive control) produced an intense vasoconstriction and haemorrhage. In contrast, 0.9 % NaCl (negative control) produced no reaction over the time tested. Similarly, the application of free bLF solution or bLF-NPs into the CAM did not expose any sign of intolerance or vascular alteration. Considering Fig. 8, it is possible to confirm the suitability for ocular administration. As a result of the study, bLF-NPs are classified as a non-irritating substance at the ocular level (Table 7). These results are in agreement to those acquired by other authors with regard to polymeric NPs and bLF loaded for ocular administration (Abrego et al., 2015; Sánchez-López et al., 2016; Varela-Fernández et al., 2021).

3.10.2. In vivo ocular tolerance of NPs

The optimized NPs formulation was evaluated using the primary irritation test or Draize test (Sánchez-López et al., 2016). Due to the sensitive nature of the eye, possible irritating effects or ocular damage, the *in vivo* ocular irritation test was of great relevance. Rabbit model are preferred to carry out this assay since its eyes are wide and well-reported physiologically, in addition to its handling and availability. Despite this advantages, its eyes are normally more predisposed to irritation than the human eye (Yousry et al., 2017). The Draize test was carried out with the certainty that each of the instilled substances has already been tested by other authors individually (Gonzalez-pizarro et al., 2019b; Sánchez-

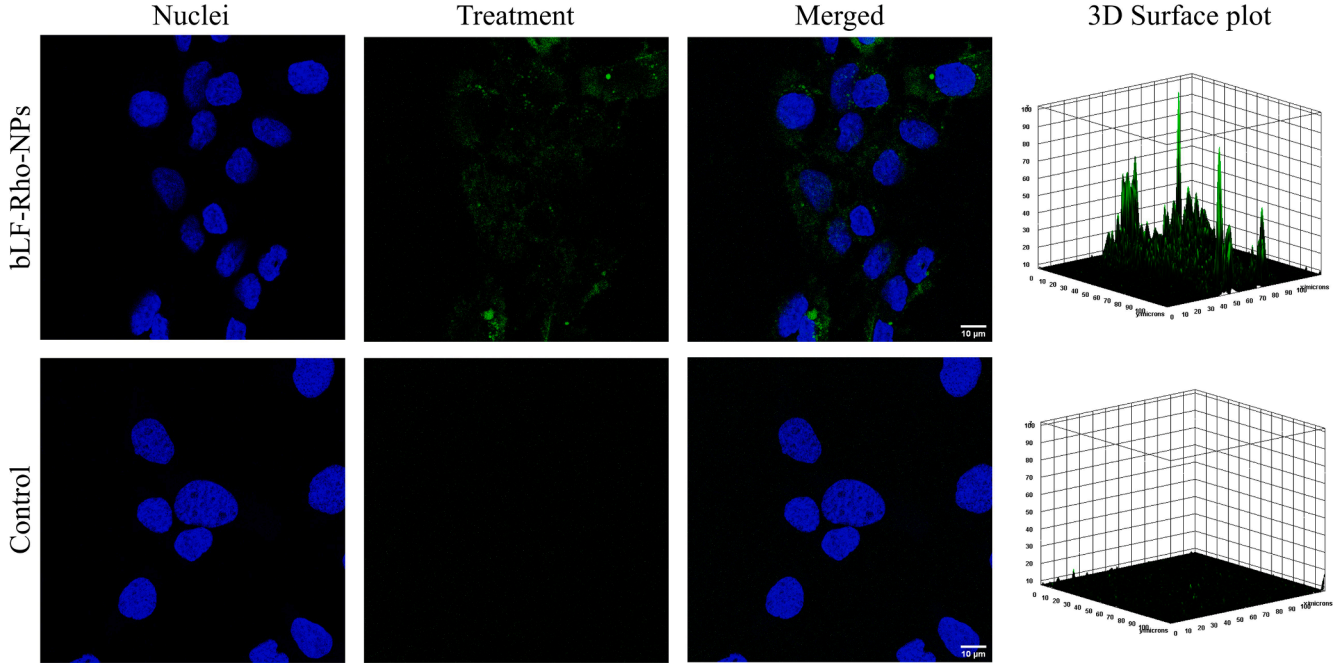

Fig 7. Cellular uptake of bLF-NPs (dilution 1:50). Images are representative of three independent biological experiments. 3D surface mapping analysis of internalized NPs (green signal).

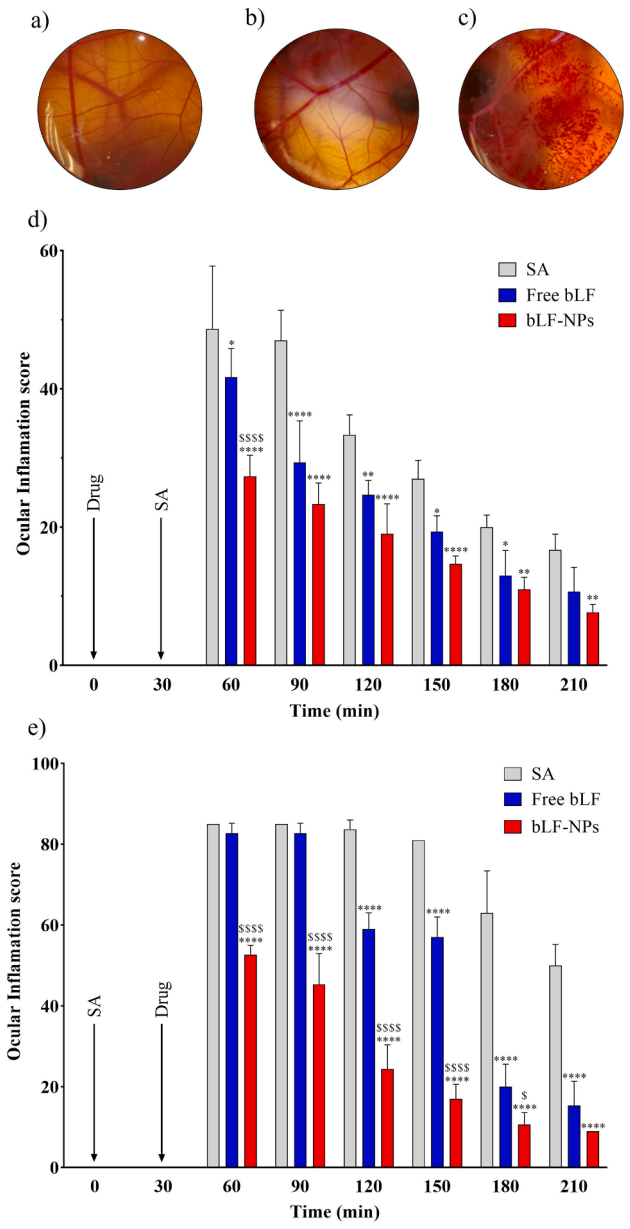

Fig. 8. HET-CAM test: (a) Free bLF; (b) bLF-NPs and (c) Positive control. (d) Ocular inflammation prevention. (e) Ocular inflammation treatment test. Values are expressed as mean ± SD; *p < 0.05, ** p < 0.01 and ***p < 0.001 and ****p < 0,0001 significantly lower than the inflammatory effect induced by SA; $p < 0.05, $$p < 0.01 and $$$p < 0.001 and $$$$p < 0,0001 significantly lower than the inflammatory effect induced by free bLF.

Table 7
In vitro ocular tolerance (HET-CAM).

Formulation	Medium score	Classification
bLF-NPs	0.07	Non-irritant
Free bLF (9.32 mg·mL^{-1})	0.07	Non-irritant

López et al., 2016). Draize test was accomplished considering the formulation safety, obtained in the previously performed *in vitro* irritation test. According to the obtained results, the total score for all rabbits was zero, without signs of ocular inflammation, redness, or increased tear production after instillation of bLF-NPs. Hence, the NPs could be classified as non-irritant substances.

3.11. *In vivo* anti-inflammatory efficacy

Two studies were carried out to determine the anti-inflammatory efficacy of the NPs, to confirm its capacity to prevent and treat ocular inflammation.

In vivo inflammatory prevention capacity of the formulations developed was evaluated. First, the formulations (bLF-NPs or free bLF) were applied, after 30 min, a drop of 0.5 % arachidonic acid (SA), the inflammation agent, was instilled. In the case of the positive control, physiological serum was administered instead of the bLF formulations. Notable differences were shown between the inflammation produced by SA and treated with bLF formulations or physiological serum. However, a slightly faster recovery and decrease in inflammation was observed in the case of those treated with bLF-NPs rather than free bLF over the time, probably due to tear clearance (Sánchez-López et al., 2016). bLF-NPs showed significant differences regarding positive control ($p < 0.0001$). Therefore, polymeric bLF-NPs exerted a preventive effect of inflammation due to the long-lasting release of bLF in the medium and its internalization on the corneal cells (Fig. 8d).

In vivo inflammatory treatment was also evaluated. Inflammation with significant hyperaemia was induced by SA after 30 min exposure (Fig. 8e). Then, bLF-NPs and free bLF were applied and the degree of inflammation was measured. It was observed that both formulations presented anti-inflammatory activity. However, the administration of bLF-NPs produced a statistically significant reduction of inflammation signs to a greater extent and faster than free bLF. This fact may be due to the improved ocular surface adherence of bLF-NPs, thus the residence time in the cornea might be longer (Sánchez-López et al., 2016). In addition, bLF-NPs also promote bLF stability in aqueous solution (Wang et al., 2019; Wang et al., 2017). Therefore, bLF-NPs prolonged release and protection exerted by the polymeric matrix might increase corneal bLF concentration producing an anti-inflammatory action that lasted for a longer period. Polymeric nanostructured systems provide an enhanced bioavailability of bLF on the ocular surface, at the corneal level, and, as previously reported, possess the ability to reach deeper tissues such as vitreous humor or retina, being beneficial in the treatment of inflammation (Bisht et al., 2017; Gonzalez-Pizarro et al., 2018).

4. Conclusions

In summary, we have developed a novel nanotechnological tool in the treatment of ocular inflammation based on the incorporation of bLF, an anti-inflammatory and antioxidant high molecular weight protein, into polymeric NPs. This controlled release system has demonstrated to be stable without signs of flocculation or precipitation. Furthermore, corneal permeability and prolonged release of the active compound has been achieved improving the pharmacokinetic and pharmacodynamic drug profile. Both *in vitro* and *in vivo* studies confirm that these systems do not present any sign of cytotoxicity or ocular irritation. Moreover, the bLF-NPs present *in vivo* anti-inflammatory efficacy either in the prevention and in the treatment of symptoms. Therefore, bLF loaded PLGA NPs constitutes a suitable system to treat and prevent ocular inflammation.

CRediT authorship contribution statement

Ana López-Machado: Conceptualization, Methodology, Investigation, Writing – original draft, Visualization. **Natalia Díaz:** Methodology. **Amanda Cano:** Formal analysis, Writing – original draft, Visualization. **Marta Espina:** Formal analysis. **Josefa Badía:** Methodology, Resources, Writing – review & editing, Funding acquisition. **Laura Baldomà:** Methodology, Resources, Writing – review & editing, Funding acquisition. **Ana Cristina Calpena:** Methodology, Formal analysis. **Martina Biancardi:** Investigation. **Eliana B. Souto:** Writing – original draft. **María Luisa García:** Conceptualization, Resources, Writing – review & editing, Funding acquisition. **Elena Sánchez-López:** Conceptualization,

Investigation, Writing – review & editing.

Declaration of Competing Interest

The authors declare that they have no known competing financial interests or personal relationships that could have appeared to influence the work reported in this paper.

Acknowledgements

This work was supported by Portuguese Science and Technology Foundation (FCT/MCT) and from European Funds (PRODER/COMPETE) under the project reference UIDB/04469/2020 (strategic found), co-financed by FEDER, under the Partnership Agreement PT2020: UIDB/04469/2020.

References

Abbouda, A., Abicca, I., Fabiani, C., Scappatura, N., Peña-García, P., Scrivo, R., Priori, R., Paroli, M.P., 2017. Psoriasis and Psoriatic Arthritis-Related Uveitis: Different Ophthalmological Manifestations and Ocular Inflammation Features. Semin. Ophthalmol. 32, 715–720. https://doi.org/10.3109/08820538.2016.1170161.

Abrego, G., Alvarado, H., Souto, E.B., Guevara, B., Halbaut, L., Parra, A., Calpena, A., Luisa, M., 2015. Biopharmaceutical profile of pranoprofen-loaded PLGA nanoparticles containing hydrogels for ocular administration. Eur. J. Pharm. Biopharm. 95, 261–270. https://doi.org/10.1016/j.ejpb.2015.01.026.

Aguilar, M., 2004. HPLC of Peptides and Proteins. Methods and Protocols, 1st ed, Methods in Molecular Biology. Humana Press, Totowa, NJ. Doi: 10.1385/1592597424.

Aketa, N., Yamaguchi, T., Asato, T., Yagi-Yaguchi, Y., Suzuki, T., Higa, K., Kurihara, T., Satake, Y., Tsubota, K., Shimazaki, J., 2017. Elevated Aqueous Cytokine Levels in Eyes With Ocular Surface Diseases. Am. J. Ophthalmol. 184, 42–51. https://doi.org/10.1016/j.ajo.2017.09.029.

Anaraki, N.I., Sadeghpour, A., Iranshahi, K., Toncelli, C., Cendrowska, U., Stellacci, F., Dommann, A., Wick, P., Neels, A., 2020. New approach for time-resolved and dynamic investigations on nanoparticles agglomeration. Nano Res. 13, 2847–2856. https://doi.org/10.1007/s12274-020-2940-4.

Andrés-Guerrero, V., Bravo-Osuna, I., Pastoriza, P., Molina-Martinez, I.T., Herrero-Vanrell, R., 2017. Novel technologies for the delivery of ocular therapeutics in glaucoma. J. Drug Deliv. Sci. Technol. 42, 181–192. Doi: 201802275371389450.

Anfuso, C.D., Olivieri, M., Fidilio, A., Lupo, G., Rusciano, D., Pezzino, S., Gagliano, C., Drago, F., Bucolo, C., 2017. Gabapentin attenuates ocular inflammation: In vitro and in vivo studies. Front. Pharmacol. 8, 1–10. https://doi.org/10.3389/fphar.2017.00173.

Bisht, R., Mandal, A., Jaiswal, J.K., Rupenthal, I.D., 2017. Nanocarrier mediated retinal drug delivery: overcoming ocular barriers to treat posterior eye diseases. Wiley Interdiscip. Rev. Nanomedicine. Nanobiotechnology e1473, 1–21. https://doi.org/10.1002/wnan.1473.

Bozdag, S., Dillen, K., Vandervoort, J., Ludwig, A., 2005. The effect of freeze-drying with different cryoprotectants and gamma-irradiation sterilization on the characteristics of ciprofloxacin HCl-loaded poly(D, L-lactide-glycolide) nanoparticles. J. Pharm. Pharmacol. 57, 699–707. https://doi.org/10.1211/0022357056145.

Cano, A., Ettcheto, M., Chang, J.H., Barroso, E., Espina, M., Kühne, B.A., Barenys, M., Auladell, C., Folch, J., Souto, E.B., Camins, A., Turowski, P., García, M.L., 2019. Dual-drug loaded nanoparticles of Epigallocatechin-3-gallate (EGCG)/Ascorbic acid enhance therapeutic efficacy of EGCG in a APPswe/PS1dE9 Alzheimer's disease mice model. J. Control. Release 301, 62–75. https://doi.org/10.1016/j.jconrel.2019.03.010.

Cano, A., Ettcheto, M., Espina, M., Auladell, C., Calpena, A.C., Folch, J., Barenys, M., Sánchez-López, E., Camins, A., García, M.L., 2018. Epigallocatechin-3-gallate loaded PEGylated-PLGA nanoparticles: A new anti-seizure strategy for temporal lobe epilepsy. Nanomedicine Nanotechnology. Biol. Med. 14, 1073–1085. https://doi.org/10.1016/j.nano.2018.01.019.

Cano, A., Sánchez-López, E., Espina, M., Egea, M.A., García, M.L., 2017. Polymeric nanoparticles of (-)-epigallocatechin gallate: A new formulation for the treatment of ocular diseases. J. Control. Release 259, e5–e195. https://doi.org/10.1016/j.jconrel.2017.03.046.

Caplan, A., Fett, N., Rosenbach, M., Werth, V.P., Micheletti, R.G., 2017. Prevention and management of glucocorticoid-induced side effects : A comprehensive review. J. Am. Acad. Dermatology 76, 201–207. https://doi.org/10.1016/j.jaad.2016.02.1241.

Carnahan, M.C., Goldstein, D.A., 2000. Ocular complications of topical, peri-ocular, and systemic corticosteroids. Curr. Opin. Ophtalmol. 11, 478–483. https://doi.org/10.1097/00055735-200012000-00016.

Carvajal-Vidal, P., Fábrega, M.J., Espina, M., Calpena, A.C., García, M.L., 2019. Development of Halobetasol-loaded nanostructured lipid carrier for dermal administration: Optimization, physicochemical and biopharmaceutical behavior, and therapeutic efficacy. Nanomedicine Nanotechnology. Biol. Med. 20, 1–10. https://doi.org/10.1016/j.nano.2019.102026.

Celia, C., Trapasso, E., Cosco, D., Paolino, D., Fresta, M., 2009. Turbiscan Lab® Expert analysis of the stability of ethosomes® and ultradeformable liposomes containing a bilayer fluidizing agent. Colloids Surfaces B Biointerfaces 72, 155–160. https://doi.org/10.1016/j.colsurfb.2009.03.007.

Chen, J., Zhou, J., Kelly, M., Holbein, B.E., Lehmann, C., 2017. Iron chelation for the treatment of uveitis. Med. Hypotheses 103, 1–4. https://doi.org/10.1016/j.mehy.2017.03.029.

Chen, X., Aqrawi, L.A., Utheim, T.P., Tashbayev, B., Utheim, Ø.A., Reppe, S., Hove, L.H., Herlofson, B.B., Singh, P.B., Palm, Ø., Galtung, H.K., Jensen, J.C.L., 2019. Elevated cytokine levels in tears and saliva of patients with primary Sjögren's syndrome correlate with clinical ocular and oral manifestations. Sci. Rep. 9, 1–10. https://doi.org/10.1038/s41598-019-43714-5.

Derouiche, M.T.T., Abdennour, S., 2017. HET-CAM test. Application to shampoos in developing countries. Toxicol. Vitr. 45, 393–396. https://doi.org/10.1016/j.tiv.2017.05.024.

Diaz-Garrido, N., Fábrega, M.J., Vera, R., Giménez, R., Badia, J., Baldomà, L., 2019. Membrane vesicles from the probiotic Nissle 1917 and gut resident Escherichia coli strains distinctly modulate human dendritic cells and subsequent T cell responses. J. Funct. Foods 61, 1–12. https://doi.org/10.1016/j.jff.2019.103495.

European Food Safety Authority, 2012. Scientific Opinion on bovine lactoferrin. EFSA J. 10, 1–26. https://doi.org/10.2903/j.efsa.2012.2701.

Fangueiro, J.F., Calpena, A.C., Clares, B., Andreani, T., Egea, M.A., Veiga, F.J., Garcia, M.L., Silva, A.M., Souto, E.B., 2016. Biopharmaceutical evaluation of epigallocatechin gallate-loaded cationic lipid nanoparticles (EGCG-LNs): In vivo, in vitro and ex vivo studies. Int. J. Pharm. 502, 161–169. https://doi.org/10.1016/j.ijpharm.2016.02.039.

Flanagan, J.L., Willcox, M.D.P., 2009. Role of lactoferrin in the tear film. Biochimie 91, 35–43. https://doi.org/10.1016/j.biochi.2008.07.007.

Foster, C.S., Kothari, S., Anesi, S.D., Vitale, A.T., Chu, D., Metzinger, J.L., Cero, O., 2016. The Ocular Immunology and Uveitis Foundation preferred practice patterns of uveitis management. Surv. Ophtalmol. 61, 1–17. https://doi.org/10.1016/j.survophthal.2015.07.001.

Fu, Y., Kao, W.J., 2010. Drug release kinetics and transport mechanisms of non-degradable and degradable polymeric delivery systems. Expert Opin. Drug Deliv. 7, 429–444. https://doi.org/10.1517/17425241003602259.

Ghasemi, H., 2018. Roles of IL-6 in Ocular Inflammation: A Review. Ocul. Immunol. Inflamm. 26, 37–50. https://doi.org/10.1080/09273948.2016.1277247.

Gómez-Segura, L., Parra, A., Calpena-Campmany, A.C., Gimeno, Á., de Aranda, I.G., Boix-Montañes, A., 2020. Ex vivo permeation of carprofen vehiculated by PLGA nanoparticles through porcine mucous membranes and ophthalmic tissues. Nanomaterials 10, 16. https://doi.org/10.3390/nano10020355.

González-chávez, S.A., Arévalo-Gallegos, S., Rascón-Cruz, Q., 2009. Lactoferrin : structure, function and applications. Int. J. Antimicrob. Agents 33, 301–308. https://doi.org/10.1016/j.ijantimicag.2008.07.020.

Gonzalez-pizarro, R., Carvajal-vidal, P., Halbault, L., Cristina, A., Espina, M., Luisa, M., 2019. In-situ forming gels containing fluorometholone-loaded polymeric nanoparticles for ocular inflammatory conditions. Colloids Surfaces B Biointerfaces 175, 365–374. https://doi.org/10.1016/j.colsurfb.2018.11.065.

Gonzalez-Pizarro, R., Parrotta, G., Vera, R., Sánchez-López, E., Galindo, R., Kjeldsen, F., Badia, J., Baldoma, L., Espina, M., García, M.L., 2019. Ocular penetration of fluorometholone-loaded PEG-PLGA nanoparticles functionalized with cell-penetrating peptides. Nanomedicine 14, 3089–3104. https://doi.org/10.2217/nnm-2019-0201.

Gonzalez-Pizarro, R., Silva-Abreu, M., Calpena, A.C., Egea, M.A., Espina, M., García, M.L., 2018. Development of fluorometholone-loaded PLGA nanoparticles for treatment of inflammatory disorders of anterior and posterior segments of the eye. Int. J. Pharm. 547, 338–346. https://doi.org/10.1016/j.ijpharm.2018.05.050.

Gu, Y., Wu, J., 2016. Bovine lactoferrin-derived ACE inhibitory tripeptide LRP also shows antioxidative and anti-inflammatory activities in endothelial cells. J. Funct. Foods 25, 375–384. https://doi.org/10.1016/j.jff.2016.06.013.

Han, F.Y., Thurecht, K.J., Whittaker, A.K., Smith, M.T., 2016. Bioerodable PLGA-based microparticles for producing sustained-release drug formulations and strategies for improving drug loading. Front. Pharmacol. 7, 1–11. https://doi.org/10.3389/fphar.2016.00185.

Hanstock, H.G., Edwards, J.P., Walsh, N.P., 2019. Tear lactoferrin and lysozyme as clinically relevant biomarkers of mucosal immune competence. Front. Immunol. 10, 1–11. https://doi.org/10.3389/fimmu.2019.01178.

Håversen, L., Ohlsson, B.G., Hahn-Zoric, M., Hanson, L.Å., Mattsby-Baltzer, I., 2002. Lactoferrin down-regulates the LPS-induced cytokine production in monocytic cells via NF-κB. Cell. Immunol. 220, 83–95. https://doi.org/10.1016/S0008-8749(03)00006-6.

Higuchi, A., Inoue, H., Kaneko, Y., Oonishi, E., Tsubota, K., 2016. Selenium-binding lactoferrin is taken into corneal epithelial cells by a receptor and prevents corneal damage in dry eye model animals. Sci. Rep. 6, 1–8. https://doi.org/10.1038/srep36903.

Iqbal, M., Zafar, N., Fessi, H., Elaissari, A., 2015. Double emulsion solvent evaporation techniques used for drug encapsulation. Intrnational J. Pharm. 496, 173–190. https://doi.org/10.1016/j.ijpharm.2015.10.057.

Kanwar, J.R., Roy, K., Patel, Y., Zhou, S., Singh, M.R., Singh, D., Nasir, M., Sehgal, R., Sehgal, A., Singh, R.S., Garg, S., Kanwar, R.K., 2015. Multifunctional Iron Bound Lactoferrin and Nanomedicinal Approaches to Enhance Its Bioactive Functions. Molecules 20, 9703–9731. https://doi.org/10.3390/molecules20069703.

Kanyshkova, T.G., Buneva, V.N., Nevinsky, G.A., 2001. Lactoferrin and Its Biological Functions. Biochem. 66, 5–13. https://doi.org/10.1023/a:1002817226110.

Kruzel, M.L., Zimecki, M., Actor, J.K., 2017. Lactoferrin in a context of inflammation-induced pathology. Front. Immunol. 8, 1–15. https://doi.org/10.3389/fimmu.2017.01438.

Lamprecht, A., Ubrich, N., Hombreiro Pérez, M., Lehr, C.-M., Hoffman, M., Maincent, P., 2000. Influences of process parameters on nanoparticle preparation performed by a double emulsion ultrasonication technique. Int. J. Pharm. 196, 177–182. https://doi.org/10.1016/S0378-5173(99)00422-6.

Lawrenson, J.G., 2018. Anterior Eye, in: Contact Lens Practice. Elsevier, pp. 10-27.e2. Doi: 10.1016/b978-0-7020-6660-3.00002-2.

Lee, J., Lee, J., Lee, S., Ahmad, T., Perikamana, S.K.M., Kim, E.M., Lee, S.W., Shin, H., 2020. Bioactive membrane immobilized with lactoferrin for modulation of bone regeneration and inflammation. Tissue Eng. - Part A 26, 1243–1258. https://doi.org/10.1089/ten.tea.2020.0015.

Li, P.C., Chen, S.C., Hsueh, Y.J., Shen, Y.C., Tsai, M.Y., Hsu, L.W., Yeh, C.K., Chen, H.C., Huang, C.C., 2021. Gelatin scaffold with multifunctional curcumin-loaded lipid-PLGA hybrid microparticles for regenerating corneal endothelium. Mater. Sci. Eng. C 120, 1–10. https://doi.org/10.1016/j.msec.2020.111753.

Liu, S., Chang, C.N., Verma, M.S., Hileeto, D., Muntz, A., Stahl, U., Woods, J., Jones, L. W., Gu, F.X., 2015. Phenylboronic acid modified mucoadhesive nanoparticle drug carriers facilitate weekly treatment of experimentallyinduced dry eye syndrome. Nano Res. 8, 621–635. https://doi.org/10.1007/s12274-014-0547-3.

Masoudipour, E., Kashanian, S., Hemati, A., Omidfar, K., Bazyar, E., 2017. Surfactant effects on the particle size, zeta potential, and stability of starch nanoparticles and their use in a pH- responsive manner. Cellulose 24, 4217–4234. https://doi.org/10.1007/s10570-017-1426-3.

Mazet, R., Yaméogo, J.B.G., Wouessidjewe, D., Choisnard, L., Gèze, A., 2020. Recent advances in the design of topical ophthalmic delivery systems in the treatment of ocular surface inflammation and their biopharmaceutical evaluation. Pharmaceutics 12, 1–55. https://doi.org/10.3390/pharmaceutics12060570.

Nekkanti, V., Marwah, A., Pillai, R., 2015. Media milling process optimization for manufacture of drug nanoparticles using design of experiments (DOE). Drug Dev. Ind. Pharm. 41, 124–130. https://doi.org/10.3109/03639045.2013.850709.

Pearlman, E., Sun, Y., Roy, S., Karmakar, M., Hise, A.G., Szczotka-Flynn, L., Ghannoum, M., Chinnery, H.R., McMenamin, P.G., Rietsch, A., 2013. Host defense at the ocular surface. Int. Rev. Immunol. 32, 4–18. https://doi.org/10.3109/08830185.2012.749400.

Pillai-Kastoori, L., Schutz-Geschwender, A.R., Harford, J.A., 2020. A systematic approach to quantitative Western blot analysis. Anal. Biochem. 593, 1–16. https://doi.org/10.1016/j.ab.2020.113608.

Ponzini, E., Scotti, L., Grandori, R., Tavazzi, S., Zambon, A., 2020. Lactoferrin concentration in human tears and ocular diseases: A meta-Analysis. Investig. Ophthalmol. Vis. Sci. 61, 10. https://doi.org/10.1167/IOVS.61.12.9.

Qaddoumi, M.G., Ueda, H., Yang, J., Davda, J., Labhasetwar, V., Lee, V.H.L., 2004. The characteristics and mechanisms of uptake of PLGA nanoparticles in rabbit conjunctival epithelial cell layers. Pharm. Res. 21, 641–648. https://doi.org/10.1023/B:PHAM.0000022411.47059.76.

Rageh, A.A., Ferrington, D.A., Roehrich, H., Yuan, C., Terluk, R., Nelson, E.F., Montezuma, S.R., 2016. Lactoferrin Expression in Human and Murine Ocular Tissue. Curr. Eye Res. 41, 883–889. https://doi.org/10.3109/02713683.2015.1075220.

Ramos Yacasi, G.R., García López, M.L., Espina García, M., Parra Coca, A., Calpena Campmany, A.C., 2016. Influence of freeze-drying and γ-irradiation in preclinical studies of flurbiprofen polymeric nanoparticles for ocular delivery using d-(+)-trehalose and polyethylene glycol. Int. J. Nanomedicine 11, 4093–4106. https://doi.org/10.2147/IJN.S105606.

Retamal Marín, R.R., Babick, F., Hillemann, L., 2017. Zeta potential measurements for non-spherical colloidal particles – Practical issues of characterisation of interfacial properties of nanoparticles. Colloids Surfaces A 532, 516–521. https://doi.org/10.1016/j.colsurfa.2017.04.010.

Rosa, L., Cutone, A., Lepanto, M.S., Paesano, R., Valenti, P., 2017. Lactoferrin : A Natural Glycoprotein Involved in Iron and Inflammatory Homeostasis. Int. J. Mol. Sci. 18, 1–26. https://doi.org/10.3390/ijms18091985.

Sah, A.K., Suresh, P.K., Verma, V.K., 2017. PLGA nanoparticles for ocular delivery of loteprednol etabonate: a corneal penetration study. Artif. Cells, Nanomedicine Biotechnol. 45, 1156–1164. https://doi.org/10.1080/21691401.2016.1203794.

Sánchez-López, E., Egea, M.A., Cano, A., Espina, M., Calpena, A.C., Ettcheto, M., Camins, A., Souto, E.B., Silva, A.M., García, M.L., 2016. PEGylated PLGA nanospheres optimized by design of experiments for ocular administration of dexibuprofen-in vitro, ex vivo and in vivo characterization. Colloids Surfaces B Biointerfaces 145, 241–250. https://doi.org/10.1016/j.colsurfb.2016.04.054.

Sánchez-López, E., Ettcheto, M., Egea, M.A., Espina, M., Calpena, A.C., Folch, J., Camins, A., García, M.L., 2017. New potential strategies for Alzheimer's disease prevention: pegylated biodegradable dexibuprofen nanospheres administration to APPswe/PS1dE9. Nanomedicine Nanotechnology. Biol. Med. 13, 1171–1182. https://doi.org/10.1016/j.nano.2016.12.003.

Sánchez-López, E., Ettcheto, M., Egea, M.A., Espina, M., Cano, A., Calpena, A.C., Camins, A., Carmona, N., Silva, A.M., Souto, E.B., García, M.L., 2018. Memantine loaded PLGA PEGylated nanoparticles for Alzheimer's disease: In vitro and in vivo characterization. J. Nanobiotechnology 16, 1–16. https://doi.org/10.1186/s12951-018-0356-z.

Schultz, C., 2018. Ocular Inflammation. Gen. Intern. Med. Clin. Innov. 3, 1–3. https://doi.org/10.15761/gimci.1000163.

Seen, S., Tong, L., 2018. Dry eye disease and oxidative stress. Acta Ophthalmol. 96, e412–e420. https://doi.org/10.1111/aos.13526.

Shalom, Y., Perelshtein, I., Perkas, N., Gedanken, A., Banin, E., 2017. Catheters coated with Zn-doped CuO nanoparticles delay the onset of catheter-associated urinary tract infections. Nano Res. 10, 520–533. https://doi.org/10.1007/s12274-016-1310-8.

Sharma, S., Parmar, A., Kori, S., Sandhir, R., 2016. Trends in Analytical Chemistry PLGA-based nanoparticles : A new paradigm in biomedical applications 80, 30–40. https://doi.org/10.1016/j.trac.2015.06.014.

Shi, J., Votruba, A.R., Farokhzad, O.C., Langer, R., 2010. Nanotechnology in Drug Delivery and Tissue Engineering : From Discovery to Applications 3223–3230. Doi: 10.1021/nl102184c.

Smith, P.K., Krohn, R.I., Hermanson, G.T., Mallia, A.K., Gartner, F.H., Provenzano, M.D., Fujimoto, E.K., Goeke, N.M., Olson, B.J., Klenk, D.C., 1985. Measurement of protein using bicinchoninic acid. Anal. Biochem. 150, 76–85. https://doi.org/10.1016/0003-2697(85)90442-7.

Soni, V., Pandey, V., Tiwari, R., Asati, S., Tekade, R.K., 2019. Design and evaluation of ophthalmic delivery formulations, in: Basic Fundamentals of Drug Delivery. Elsevier Inc., pp. 473–538. Doi: 10.1016/B978-0-12-817909-3.00013-3.

Suzuki, Y., Wong, H., Ashida, K., Schryvers, A.B., Lönnerdal, B., 2009. The N1 Domain of Human Lactoferrin is Required For Internalization By Caco-2 Cells and Targeting to the Nucleus. Biochemistry 47, 10915–10920. https://doi.org/10.1021/bi8012164.The.

Talluri, R.S., Hariharan, S., Karla, P.K., Mitra, A.K., 2010. Drug delivery to cornea and conjunctiva: Esterase- and protease-directed prodrug design, in: Encyclopedia of the Eye. Elsevier, Kansas City, pp. 42–53. Doi: 10.1016/B978-0-12-374203-2.00080-4.

Tamhane, M., Cabrera-Ghayouri, S., Abelian, G., Viswanath, V., 2019. Review of Biomarkers in Ocular Matrices: Challenges and Opportunities. Pharm. Res. 36, 1–35. https://doi.org/10.1007/s11095-019-2569-8.

Tao Meng, F., Hui Ma, G., Qiu, W., Guo Su, Z., 2003. W/O/W double emulsion technique using ethyl acetate as organic solvent: effects of its diffusion rate on the characteristics of microparticles. J. Control. Release 91, 407–416. Doi: 10.1016/s0168-3659(03)00273-6.

Tapia-Guerrero, Y.S., Del Prado-Audelo, M.L., Borbolla-Jiménez, F.V., Giraldo Gomez, D. M., García-Aguirre, I., Colín-Castro, C.A., Morales-González, J.A., Leyva-Gómez, G., Magaña, J.J., 2020. Effect of UV and gamma irradiation sterilization processes in the properties of different polymeric nanoparticles for biomedical applications. Materials (Basel). 13, 1–19. https://doi.org/10.3390/ma13051090.

Varela-Fernández, R., García-Otero, X., Díaz-Tomé, V., Regueiro, U., López-López, M., González-Barcia, M., Lema, M.I., Otero-Espinar, F.J., 2021. Design, Optimization, and Characterization of Lactoferrin-Loaded Chitosan/TPP and Chitosan/Sulfobutylether-β-cyclodextrin Nanoparticles as a Pharmacological Alternative for Keratoconus Treatment. ACS Appl. Mater. Interfaces 13, 3559–3575. https://doi.org/10.1021/acsami.0c18926.

Vega, E., Egea, M.A., Calpena, A.C., Espina, M., García, M.L., 2012. Role of hydroxypropyl- β -cyclodextrin on freeze-dried and gamma-irradiated PLGA and PLGA – PEG diblock copolymer nanospheres for ophthalmic flurbiprofen delivery. Int. J. Nanomedicine 7, 1357–1371. https://doi.org/10.2147/IJN.S28481.

Wadhwa, S., Paliwal, R., Paliwal, S., Vyas, S., 2009. Nanocarriers in Ocular Drug Delivery: An Update Review. Curr. Pharm. Des. 15, 2724–2750. https://doi.org/10.2174/138161209788923886.

Wang, B., Timilsena, Y.P., Blanch, E., Adhikari, B., 2019a. Lactoferrin: Structure, function, denaturation and digestion. Crit. Rev. Food Sci. Nutr. 59, 580–596. https://doi.org/10.1080/10408398.2017.1381583.

Wang, B., Timilsena, Y.P., Blanch, E., Adhikari, B., 2017. Characteristics of bovine lactoferrin powders produced through spray and freeze drying processes. Int. J. Biol. Macromol. 95, 985–994. https://doi.org/10.1016/j.ijbiomac.2016.10.087.

Wang, T., Markham, A., Thomas, S.J., Wang, N., Huang, L., Clemens, M., Rajagopalan, N., 2019b. Solution Stability of Poloxamer 188 Under Stress Conditions. J. Pharm. Sci. 108, 1264–1271. https://doi.org/10.1016/j.xphs.2018.10.057.

Ward, P.P., Paz, E., Conneely, O.M., 2005. Multifunctional roles of lactoferrin : a critical overview. Cell. Mol. Life Sci. 62, 2540–2548. https://doi.org/10.1007/s00018-005-5369-8.

Yan, F., Zhang, C., Zheng, Y., Mei, L., Tang, L., Song, C., Sun, H., Huang, L., 2010. The effect of poloxamer 188 on nanoparticle morphology, size, cancer cell uptake, and cytotoxicity. Nanomedicine Nanotechnology. Biol. Med. 6, 170–178. https://doi.org/10.1016/j.nano.2009.05.004.

Yao, X., Bunt, C., Cornish, J., Quek, S.Y., Wen, J., 2014. Preparation, optimization and characterization of bovine lactoferrin-loaded liposomes and solid lipid particles modified by hydrophilic polymers using factorial design. Chem. Biol. Drug Des. 83, 560–575. https://doi.org/10.1111/cbdd.12269.

You, J., Yu, Y., Cai, K., Zhou, D., Zhu, H., Wang, R., Zhang, Q., Liu, H., Cai, Y., Lu, D., Kim, J.K., Gan, L., Zhai, T., Luo, Z., 2020. Enhancement of MoTe2 near-infrared absorption with gold hollow nanorods for photodetection. Nano Res. 13, 1636–1643. https://doi.org/10.1007/s12274-020-2786-9.

Yousry, C., Elkheshen, S.A., El-laithy, H.M., Essam, T., Fahmy, R.H., 2017. Studying the influence of formulation and process variables on Vancomycin-loaded polymeric nanoparticles as potential carrier for enhanced ophthalmic delivery. Eur. J. Pharm. Sci. 100, 142–154. https://doi.org/10.1016/j.ejps.2017.01.013.